University of Alberta

A Parametric Study of a Flash Atomized Spray Using PDPA

by

Kevin Breton

A thesis submitted to the Faculty of Graduate Studies and Research
in partial fulfillment of the requirements for the degree of

Master of Science

Department of Mechanical Engineering

Contents

List of Figures

List of Tables

Nomenclature

Symbol	Definition		Dimension
a	Sonic velocity		[m/s]
D	Nozzle diameter		[m]
D_f	PDPA fringe spacing		[m]
D_g	Geometric mean diameter		[m]
D_{32}	Sauter mean diameter		[m]
D_p	Droplet diameter		[m]
f_D	Doppler frequency		$[s^{-1}]$
h	Enthalpy		[kJ/kg]
L	Nozzle length		[m]
n_{droplet}	Droplet index of refraction		[−]
n_{medium}	Medium index of refraction		[−]
n_{rel}	Relative index of refraction	$n_{\text{rel}} = n_{\text{droplet}}/n_{\text{medium}}$	[−]
$\bar{N}$	Normalized PDPA data rate		[−]
P_{res}	Reservoir pressure		[Pa]
P_{amb}	Ambient pressure		[Pa]
p_r	Pressure ratio	$p_r = P_{\text{res}}/P_{\text{amb}}$	[−]
r	Radial position		[m]
S	Slip ratio		[−]
T_{res}	Reservoir temperature		[°C]
T_{sat}	Saturation temperature		[°C]
ΔT_{SH}	Degree of superheat	$\Delta T_{SH} = T_{\text{res}} - T_{\text{sat}}$	[°C]
U_z	Axial droplet velocity		[m/s]
x	Steam quality		[−]
z	Axial position		[m]
α	Void fraction		[−]
ϵ	Uncertainty		[−]
θ	PDPA beam angle		[°]
θ_n	Near-field spreading angle		[°]
θ_f	Far-field spreading angle		[°]
λ	Wavelength		[m]
μ_{D_p}	Average particle diameter		[m]
ρ	Density		[kg/m^3]
σ_{D_p}	Standard deviation of droplet diameters		[m]
σ_g	Geometric standard deviation		[−]
ϕ	PDPA receiver angle		[°]
ψ	PDPA emitter viewing angle		[°]

Chapter 1

Introduction

1.1 Flash Atomization Process

Flash atomization is a thermodynamic process by which a dispersed spray of droplets is produced. This process occurs when a liquid, maintained at a temperature and pressure which renders it super-heated relative to the ambient, is introduced rapidly into ambient conditions. The thermodynamic process is illustrated in Figure 1.1.

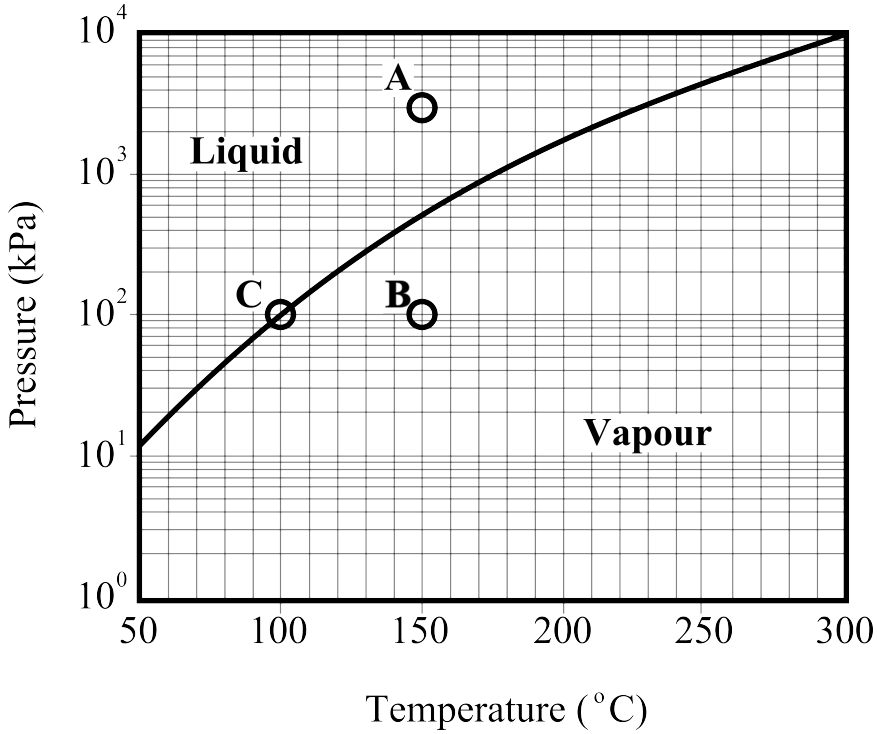

Figure 1.1: Phase diagram of water. Points A, B, and C represent the state of the fluid prior to, during, and following the release, respectively.

This phase diagram in Figure 1.1 illustrates the process which occurs as the super-heated liquid is released. This diagram assumes that the release occurs iso-thermally. Given the

short transit time of the fluid, this model will be used to gain a general understanding of the phenomenon. As the pressure undergoes a rapid drop (from point A to B on Figure 1.1), the liquid is no longer in a thermodynamically stable state. At point B, representing the state of the fluid immediately after release, the pressure and temperature indicate that the stable state is vapour. In order to achieve thermodynamic equilibrium, a portion of the liquid boils rapidly, resulting in a two phase mixture of saturated vapour at point C. The system returns to a thermodynamically stable state as the latent heat of the phase change process removes excess energy from the remaining liquid state (Vetrano *et al.* (2012)). Given the large density ratios between liquid and vapour phases ($(\rho_l/\rho_g)_{H_2O} \approx 1600$), even for low mass fractions of vapour, the void fraction is large.

The onset of the phase change process occurs at nucleation sites. It is at these locations that the meta-stable liquid can form a vapour bubble which consequentially grows until the system is once again stable. As reported by El-Fiqi *et al.* (2007), these nucleation sites may be in the form of dissolved gases or impurities, or surface roughness of the outer walls of the pipe or nozzle. Following the onset of nucleation, the process enters the bubble growth phase. With the phase change process initiated, the continued boiling continues until the latent heat absorbed by converting the liquid to a vapour is balanced by the excess energy of the liquid which initially rendered it thermodynamically unstable. As the liquid is broken up into smaller droplets, the effects of surface tension become significant. For small drops, the effect of the surface tension is to increase the internal pressure of the droplet beyond the ambient pressure. As a result, the saturation temperature of small droplets is larger than that of large droplets. The complex process of nucleation and bubble growth is treated in greater detail by Sher. *et al.* (2008).

1.2 Other Atomization Techniques

Given the ubiquity of atomized sprays in a variety of technical fields, there exists many means by which an atomized spray can be produced. Numerous mechanisms exist in order to achieve atomization with a wide variety of fuels and under a broad range of operating conditions.

A simple form of atomization uses pressure atomizers. These systems spray a single component liquid jet under high pressure into an ambient medium. Turbulent structures within the liquid jet enhance the entrainment of the ambient medium and the large velocity ratio between the jet and the ambient provides sufficient shear forces to produce atomized droplets (Kolev (2005)). This type of atomization does not require the introduction of the

gas phase into the liquid prior to the nozzle outlet. The mixing occurs downstream of the nozzle outlet as the high velocity liquid interacts with the stationary ambient. This is a stagewise process, with the breakup of the liquid jet occurring from the free surface inwards (Brennen (2005)). This type of atomization is commonly used in Diesel engine injectors. Payri *et al.* (2012) note four separate breakup regimes of this type of spray, dependant upon the relative velocity of the jet and ambient. At high velocities, the breakup of the jet occurs next to the nozzle outlet. Pressure atomizers of this type are capable of producing fine atomization, with $D_{32} \approx 10\,\mu\text{m}$, according to Dernotte *et al.* (2012). However, in order to achieve this level of atomization, high pressure differences of up to 150 MPa are required. It is noted by Dernotte *et al.* (2012), however, that as the pressure difference is increased, the penetration length is also increased. Furthermore, the D_{32} values produced by such systems are positively correlated with the fuel viscosity (Dernotte *et al.* (2012)). This fact indicates that the atomization of high viscosity fuels is better suited to alternative systems.

Another atomization technique common in industrial applications is effervescent atomization. This is a technique similar to flash atomization. Gas is introduced into the liquid flow upstream of the nozzle. As the pressure drops through the nozzle, these gas expands and creates liquid ligaments which are further broken up by the effects of the bubble break up and shear forces within the jet, (Jedelsky and Jicha (2012)). This type of atomization is common within the heavy oil industry, where high temperature steam is injected into a high viscosity bitumen flow in order to produce an atomized spray (Rahman *et al.*, (2012)). This type of atomizer was developed in order to produce effective atomization of unconventional hydrocarbons (Konstantinov *et al.* (2010)). It is noted by Konstantinov *et al.* (2010) that effervescent atomization results in a decreased dependency on fluid viscosity, thereby enabling the use of a single atomizing nozzle for a variety of fuels and applications. This type of atomization is highly dependent on the operating conditions. It was found by Sarkar and Ramamurthi (2007) that the flow regime of effervescent atomizers is dependent on both the Reynolds number of the flow as well as the gas to liquid ratio. A change on the flow regime (eg. from bubbly flow to slug flow) can result in significant changes in the spray characteristics downstream of the nozzle. This is an undesirable trait, particularly in situations where constant, steady operating conditions are not guaranteed. Additionally, despite improved effectiveness compared to other atomization techniques in terms of dependence on the fluid viscosity, Ferreira *et al.* (2001) note that the spray characteristics of effervescent atomization still exhibit significant dependance on the fluid viscosity.

Large molecular weight hydrocarbons typically posses a large viscosity. This makes

the atomization of such fuels difficult with conventional systems. Large scale fluid cokers used in heavy oil applications utilize effervescent atomizers by injecting high temperature steam into the bitumen flow (Rahman *et al.* (2012)). There may be the possibility of improving the efficiency of this process using flash atomization. Due to the compressibility effects, there are comparatively large energy expenditures in pressurizing steam (as in the industrial fluid cokers) compared single phase liquids. Using flash atomization, it may be possible to create a long chain hydrocarbon suspension in a single phase liquid. The liquid component can then be boiled into vapour via the flashing process leaving only the fuel particles in a dispersed spray.

1.3 Literature Review

Flash atomization is a phenomenon that is well documented in the scientific literature. However, Sher *et al.* (2008) state that the limited fundamental understanding of the flash atomization process has limited its use in a variety of possible areas. To fill this knowledge gap, various researchers have studied aspects of the flash atomization process. A wide array of experimental techniques have been employed under numerous operating conditions. This section will outline the fields, methodologies, and results of published literature in the field of flash atomization.

1.3.1 Applications

As opposed to many typical atomization techniques which rely on shear forces to produce an atomized spray, flash atomization is driven by the phase change of the fluid. This provides many challenges and opportunities for the implementation of flash atomization. The continued study of the flash atomization process may lead to incremental improvements in energy systems and the reduction of hydrocarbon related pollutant emissions (Kim *et al.* (2012)).

Much of the research involves the flash atomization of binary liquid mixtures. In these scenarios, a two component mixture of liquids is prepared in which one of the components flashes at a lower temperature than the other. After the flashing process, a two phase spray is obtained from the original single phase mixture. The component of the mixture with the lower flashing temperature boils rapidly into a dispersed vapour phase while the remainder of the liquid is dispersed by the rapid expansion of the flashing component. Such systems were studied by Zhang *et al.* (2005) as well as Sher and Zeigerson-Katz (1996). These mixtures allow for a single phase mixture to be converted into a two phase spray.

Compared to many conventional atomization techniques, flash atomization produces a spray with a large effective spray angle and minimized penetration depth, (Park and Lee, 1994). Because the atomization is initially produced by the flashing mechanism instead of shear forces, flash atomization does not require very large velocity gradients. This reduced inertia minimizes the penetration depth of the spray into the ambient medium and also allows for a larger effective spray angle. These characteristics render flash atomization a potentially useful phenomenon in the field of combustion systems and fuel injectors. Li *et al.* (2012) have studied the potential of flash atomization in diesel fuel injectors. Diesel fuel blended with Dimethyl Ether (DME) was tested using a flash atomizing nozzle. DME concentrations of 10% and 20% by weight were used in this study. Yu *et al.* (2010a) and Yu *et al.* (2010b) studied the use of DME blended fuel in homogenous charge compression ignition engines. These technologies have the potential to significantly lowering both the particulate and nitrogen oxide (NO_x) emission(Yu *et al.* (2010a))

An interesting distinction was raised by Aleiferis and Romunde (2013) who studied various fuels in a multi hole injector for a spark ignition engine. They noted that under hot conditions and at low load (therefore lower receiver pressure), flash atomization may occur in the injectors of spark ignition engines. Though the onset of flash atomization results in higher dispersion of the fuel droplets, it can be undesirable in spark ignition engines since the high dispersion and low penetration depth result in "spray collapse" and the destruction of the directionality of the spray. Given the lower injector pressures used in spark ignition engines as opposed to diesel engines, the onset of "spray collapse" occurs more readily. At present, the more active area of research is into using flash atomization in diesel injectors.

Another potential avenue of research involving flash atomization is for the spray and combustion of coal and water suspensions. This work was studied by Yu and Beer (1998). More recently, Kim *et al.* (2012) investigated the effectiveness of using flash atomization to improve the spray characteristics of a heavy oil emulsion used in a swirl injector. The emulsified heavy oil results in a significantly reduced viscosity and, combined with improved atomization techniques, allows for the utilization of heavy oils as a fuel source while mitigating many often associated pollutant problems.

In hydrocarbon suspension systems, the fuel droplet size can be made to be a property of the suspension. In this case, there exists the potential to decouple the spray droplet diameter from the operating pressure. Since the fuel particle size is determined by the suspension properties (eg. fuel droplet size and concentration), the fuel particle size can be prescribed, provided that there exists sufficient energy to initiate the flash atomization

process. This type of system has potential benefits; by decoupling the droplet size from the upstream pressure, the spray characteristics may be only minimally affected by changes in operating pressure or flow rates or physical scale up. This is a beneficial characteristic in power generating systems, where demand fluctuates and typical atomizers lose efficiency when the flow rate deviates significantly from the design point.

1.3.2 Methodology in Literature

There are many different measurement techniques used in the study of flash atomized sprays. There are also many difficulties in gathering measurements in the dense spray environment produced by many flash atomization systems. The nature of the desired data will often dictate the type of measurement system used.

An early, yet persisting method of measuring dispersed sprays is the use of shadowgraphy. A short exposure photograph is taken of a back-lit spray. This method can be used to measure aggregate spray characteristics and works well even in dense sprays. Kamoun *et al.* (2010) used high speed shoadowgraphy with a 1 µs camera exposure in order to measure the effect of reservoir conditions on the spray angle and lateral spreading of a flash atomized spray. Kim *et al.* (2012) used a similar type of system with a $7 - 10$ ns exposure with a high intensity back light. A 1 000 frame per second high speed video camera was used by Zhifou *et al.* (2012) in order to characterise the spray produced by a flashing R134a jet. With proper magnification and equipment, Li *et al.* (2012) used a 10 µs flash in order to measure individual droplet diameters. A drawback of this method is that detailed droplet diameter measurements can be difficult to obtain and require the use of advanced software for data processing.

Given that the temperature of the pressurized liquid and subsequent dispersed spray is an important parameter in determining the spray characteristics, there has been significant research into measuring the temperature field of flash atomized sprays. Zhifou *et al.* (2012) measured the average droplet temperature of an R134a jet using a custom designed type-T thermocouple probe. In order to obtain a sufficient level of spatial resolution, many successive thermocouple measurements were taken at various axial and radial positions. In measuring the effect of temperature on the mass flow rate of a flashing jet, Rossmeissl and Wirth (2006) used thermocouples embedded in the nozzle, as well as an additional thermocouple on the spray axis 1 mm downstream of the nozzle. The use of thermocouples is limited by both the response time of the measurement and the need for a contact measurement. The mass of the thermocouple impacts the response time and in sprays with

significant thermal gradients in time, the use of thermocouples may only read the spatially averaged values. Furthermore, in investigating the temperature distribution of a flashing jet, Vetrano at. al. (2012) noted that intrusive measurements, such as the use of thermopcouples, can trigger the flashing of the spray earlier than would otherwise happen. It was noted that instruments such as rake thermocouples may be used in the fully developed region of the flow, downstream of the nozzle, but a non-intrusive system is required in the near field region.

In order to achieve a large field temperature measurement, Vetrano *et al.* (2012) used planar laser induced fluorescence (PLIF) in order to determine the temperature of the spray over a large area. PLIF measurements show a temperature dependence in the fluorescent light emitted and can therefore be used in order to measure the droplet temperature in the measurement plane. The use of PLIF measurements is limited, however, due to high sensitivity to spatial alignment and low signal strength from small droplets. This study used a pulsed Nd:YAG laser and a two camera system to measure the temperature. This system used allowed for the measurement of the droplet temperature from the nozzle outlet to a position 144 mm downstream. Because this is a non-intrusive measurement, the flow field remained undisturbed.

Laser based systems are also widely used in order to collect droplet velocity and diameter data from flash atomized sprays. There are many different types of optical measurement systems, each with certain benefits and limitations. Yu and Beer (1998) used a laser diffraction analyzer in order to measure the droplet diameter in their coal suspension spray. Another similar system is the Malvern particle sizer, used by Park and Lee (1994) in order to obtain diameter measurements of a developing flash atomized flow. The Malvern particle sizer provides the diameter distribution of particles passing through the measurement volume. Lecourt and Barricau (2009) used both particle image velocimetry (PIV) and a Malvern particle sizer to analyze flash atomized sprays. The particle sizer used in their study provides the diameter distribution over a large spatial volume (135 mm by 10 mm diameter cylinder). This prevented a detailed analysis of the spatial variance in the droplet distribution. The PIV system provides the particle velocity over a large spatial area, though it can be difficult to use in dense sprays. Aleiferis and Romunde (2013) used both a Malvern particle sizer and a phase Doppler particle analyzer (PDPA) system in studying the flashing of a two component fuel in a direct injection engine. The PDPA system provides concurrent velocity and diameter data, though only localized at the relatively small measurement volume.

The use of optical measurement systems in flash atomizing systems can be complicated by the nature of the spray. A high spray density can limit the optical transparency of the spray. In these cases, the data rate from most optical systems diminishes. Higher laser power and tuned optics can be used to mitigate these problems, but the issue persists. This problem was encountered by Hervieu and Veneau (1996), whose research necessitated the use of protections to limit the spray density in the measurement region. In order for the PDPA system to provide sufficient signal, obstructions were placed that blocked the majority of the flow and introduced errors of up to 40% in velocity measurements and 20% in diameter measurements. Yidliz et. al. (2004) studied the feasibility of various laser based measurement techniques in flash atomization research and found that, while useful, PDPA measurements are subject to some limitations. First, spray measurements in the near field of the nozzle outlet were complicated by the relatively high concentration of large, non-spherical ligaments in the flow. These ligaments are rejected by the PDPA system and the data rate declines. Furthermore, Yidliz et. al (2004) noted that in order to limit the overall spray density, the flow rate had to be limited. Doing so allowed for sufficient optical transparency in the spray for PDPA measurements.

1.3.3 Results in Literature

Flash atomization systems have demonstrated the ability to produce fine, dispersed sprays in a manner that is competitive with other atomization methods. The research focus has been broad and a wide variety of results have been collected.

An important parameter in many sprays is the spray angle and width of the spray envelope. These parameters influence the degree to which the spray mixes with the ambient fluid. This is of considerable importance in combustion applications where sufficient mixing with the ambient air is required for optimal performance. Kamoune *et al.* (2010) tested the effect of the degree of superheat on the spray angle in flash atomized sprays. It was found that when the liquid is not super-heated, or only super-heated to low levels, the spray formation is dominated by mechanical breakup. Once the onset of flashing begins, the spray angle increases rapidly and exhibits a positive correlation with the degree of super-heat. This effect was also observed by Kim *et al.* (2012) in studying the effect of flash boiling in emulsified heavy oils. Park and Lee (1994) studied the effect of liquid temperature on the spray angle as well. These results indicated that increasing temperatures results in increased spray angles , but only for a certain temperature range. Beyond a certain temperature, the spray angle remains relatively constant or decreases. This effect is explained as being a

balance of enhanced atomization at high temperatures, resulting in smaller droplets with larger radial velocities, and with the increased effect of air entrainment on small droplets.

The velocity profiles of flashing sprays have also been studied in detail. In studying a flashing R134a spray, Zhifu *et al.* (2012) measured the velocity profiles a variety of axial distances from the nozzle outlet. it was found that the velocity profiles were Gaussian in shape and that the centerline velocity decreased at larger axial distances. As the spray envelope increased in the downstream direction, the velocity profile became increasingly uniform. Yildiz *et al.* (2006) found that, as in single phase jets, the maximum velocity at a given axial location is located on the jet centerline. It was also noted that while the droplet velocities decreased in the radial direction, the root-mean-squared (RMS) of the velocities increased, indicating increased fluctuations.

Another important parameter in the measurement of spray systems is the droplet diameter produced by the spray. In reactive flows, this parameter is of vital importance. In studying DME blended diesel fuel, Li *et al.* (2012) found that as the mass percentage of DME in the fuel increased resulted in decreased droplet diameters. The authors attributed this decrease in diameter to the flash boiling of the DME in the injector system. Lecourt and Barricau (2009) studied the flashing phenomenon in a single fluid spray. Their work found negative correlations between the Sauter mean diameter and the degree of superheat. These correlations were consistent across a variety of nozzles and the general effect of upstream super-heat on the diameter distribution was posited to be independent of nozzle type. Zhang *et al.* (2005) found that, like in other forms of atomization, delivery pressure can also influence the droplet size. In their study, it was found that increased injection pressures resulted in decreased values of the Sauter mean diameter. The tests performed operated at high pressures of up to 8 MPa. Decreased droplet diameter results in a larger surface area to volume ratio. as this ratio increases, so does the reaction rate in combustion process. In applications with combustion, by reducing the reaction time, complete combustion can occur more rapidly and pollutant emissions may be reduced. Sher *et al.* (1996) state that a flash atomized spray can be used in fuel injectors in order to achieve comparable fuel atomization with lower injector pressures.

1.4 Hypothesis

The current literature does not highlight a detailed study of the effects of the degree of superheat at a variety of pressure levels, particulary over a broad range of both parameters. The relationship between superheat and the droplet velocities and diameters has been mea-

sured, but the evolution of this relationship as the pressure ratio is increased is, as of yet, unknown. The current study aims to explore the effects of both parameters, pressure ratio, p_r (The ratio of the reservoir pressure to atmospheric pressure) and degree of superheat ΔT_{SH} (The difference between the reservoir temperature and the saturation temperature at atmospheric conditions), on the droplet characteristics of a flash atomized spray. Unlike many conventional atomization systems where pressure dependance dominates, flash atomization has been shown to be strongly dependant on the degree of superheat. The current study aims to determine if the temperature dependance dominates, and the spray produced is relatively robust with respect to changes in the pressure, and if so, at what degree of superheat does this robustness occur.

Chapter 2

Experimental Setup and Methodology

2.1 Experimental Setup

The flash atomization research was performed in the combustion and sprays laboratory in the Department of Mechanical Engineering at the University of Alberta. The experiments were performed from January to October 2012. A schematic of the flash atomizing system can be found in Figure 2.1. This schematic denotes the important auxiliaries attached to the pressure vessel.

Locations of temperature and pressure measurement are denoted by the T and P symbols respectively A ball valve was used immediately upstream of the nozzle in order to control the spray. This schematic also illustrates the angle of the PDPA receiver relative to the axis of the PDPA emitter. An angle of 30 ° was chosen. Using water with a refractive index of 1.33, the angle of 30 ° provides a strong signal in the forward scatter mode. The signal is received via the first order refraction of the laser light through the water droplets.

In this study, liquid water was used as the flashing fluid. The water was contained within a cylinder and pressurized using a regulated N_2 bottle. The regulator used allowed for a maximum pressure of approximately 1.75 MPa. Because the N_2 supply is constant, even whilst the liquid is spraying, the upstream pressure of the fluid fluctuates minimally. This is a benefit over other flash atomization system with utilize a pressurized container of some flashing fluid (eg. R134a). In these scenarios, as the flashing fluid is utilized, the upstream pressure decreases. This results in an unsteady state spray [29].

In order to provide the energy required to superheat the liquid water, three (3) 200 W band heaters were placed around the hydraulic cylinder. The portion of the cylinder not heated was insulated in order to minimize heat loss and internal temperature gradients in

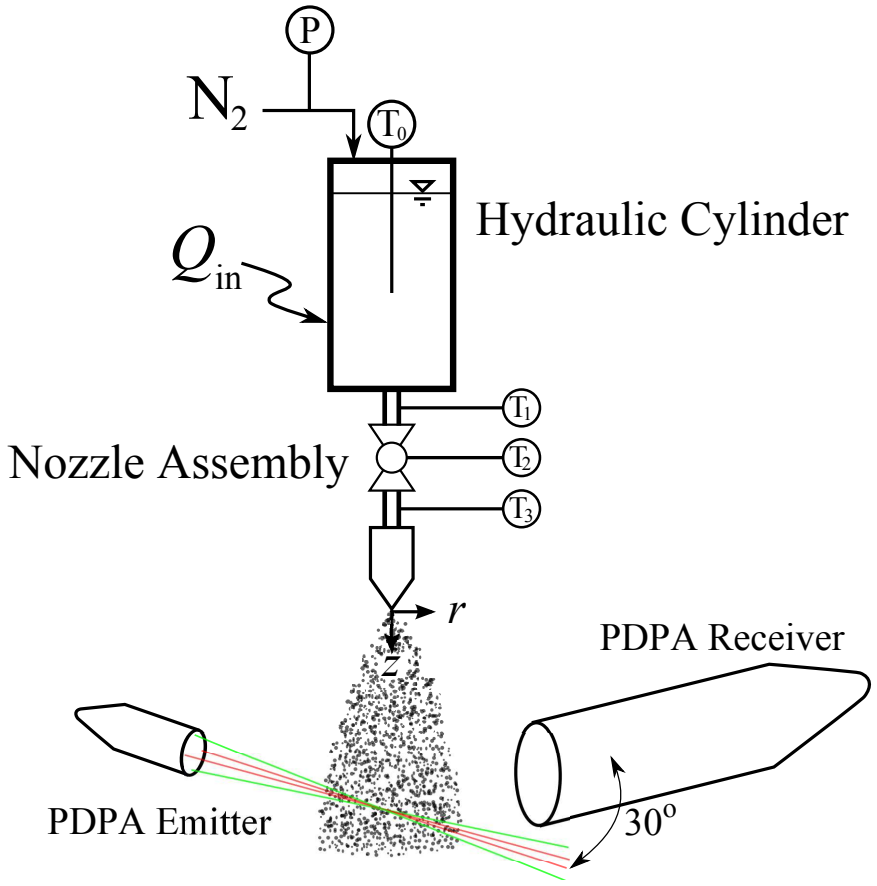

Figure 2.1: Schematic of spray subsystem with PDPA measurements

the water. The temperature of the water was measured using a type J thermocouple probe inserted into the hydraulic cylinder.

In this experiment, the release of the liquid was designed to be adiabatic. In order to limit the heat loss of the fluid as it passes through the nozzle assembly, the valve, nozzle, and pipe downstream of the hydraulic cylinder were pre-heated with a 120 W flexible band heater. Three (3) surface mounted type T thermocouples were used in order to measure the temperature along the nozzle assembly. During experiments, a maximum allowable deviation of 5 °C from the reservoir temperature was used for the nozzle assembly. The nozzle temperature was maintained throughout the release of the flashing fluid in order to maintain a relatively constant exit temperature. In Appendix B, the heat transfer within the nozzle assembly is modeled. It was found that the outlet temperature varies by less than 5 °C for variations in the surface temperature of up to 10 °C. By minimizing the temperature gradients along the flow direction, the model of an adiabatic process is validated. All pressure and temperature transducers were connected to a National Instruments data

acquisition card to allow for the accurate and concurrent measurement of all values.

Long exposure images of the flashing spray were also collected. This was done using a commercial CCD camera (Canon Rebel XTi). The setup used for imaging the spray is shown in Figure 2.2. An incandescent light source was used in a back scatter configuration in order to obtain the 30 s exposure images.

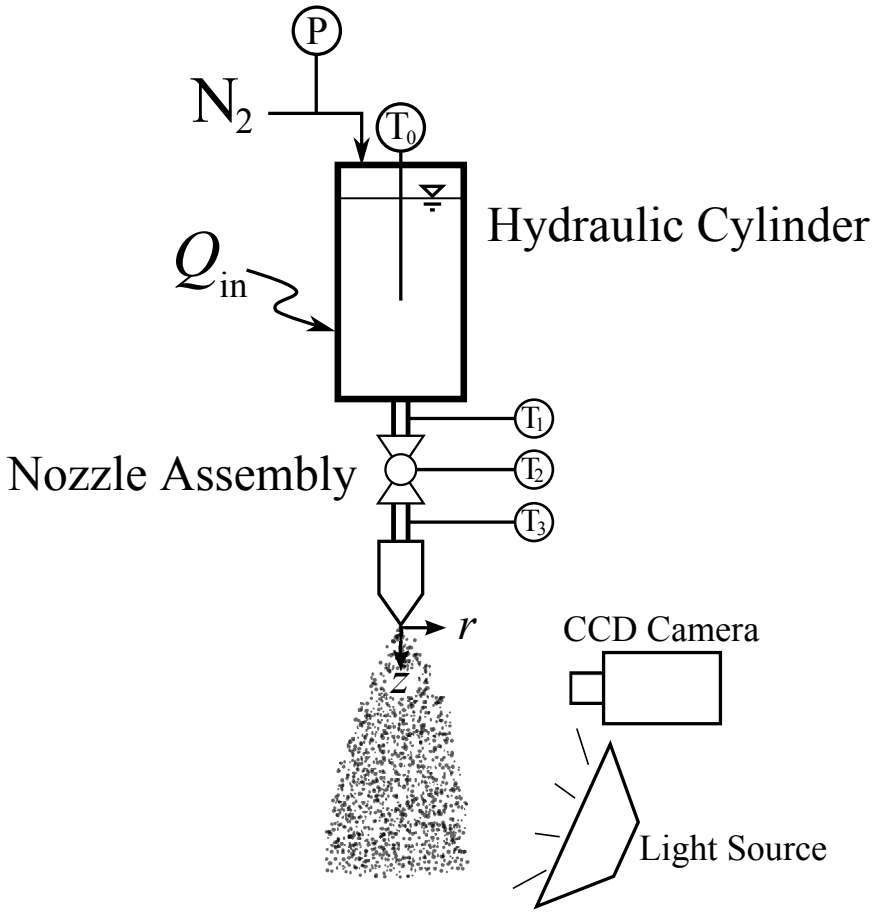

Figure 2.2: Schematic of spray subsystem with long exposure images

A solid model of the experimental was made in order to illustrate the setup of the entire system. This model is shown in Figure 2.3. A hydraulic cylinder was used in order to contain the flashing fluid at the required temperature and pressure. This vessel was mounted on a cantilevered steel frame over a plastic collector basin. A lid over the collector basin provided a means to apply a small negative pressure to the collector basin. This was done in order to collect the spray droplets downstream of the measurement location so as to prevent any obstruction of the optical measurement system. This negative pressure was applied with a small industrial vacuum. As shown in Figure 2.3, the PDPA receiver and emitter were mounted aluminium optical rails that were attached to a motorized three axis

traverse system (Schridtmotor C-104). This computer controlled traverse systems allows for the movement of the measurement volume in three spatial axes. Because both the emitter and receiver were mounted to the traverse on rigid optical rails, any translation maintained the relative position and orientation between the emitter and receiver. This allows for the measurement of the droplet properties at a variety of spatial positions during an individual flashing release. Due to the high spray density near the nozzle outlet, PDPA measurements were made along a plane an axial distance of $z = 150\,\text{mm}$ from the nozzle outlet. At this position, the PDPA data rates were sufficiently high in order to acquire data across the entire radial profile during a single experimental release.

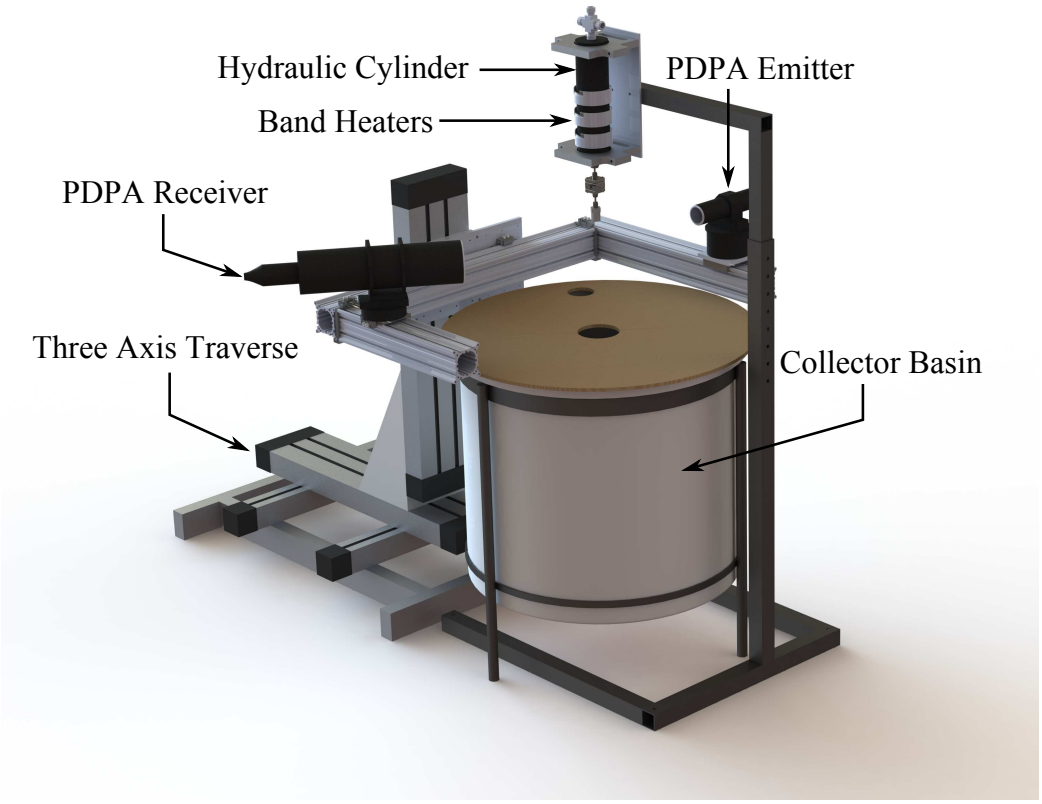

Figure 2.3: Solid model of experimental setup

Velocity and diameter measurements were made using a phase Doppler particle analyzer (Dantec FlowLite 2D). This non-intrusive laser based measurement system allows for the concurrent measurement of the 2-dimensional velocity as well as the droplet diameter. The Dantec PDPA uses a 10 mW He-Ne laser ($\lambda = 632.8\text{nm}$) and a 10 mW Nd:YAG laser ($\lambda = 532\text{nm}$). A schematic illustrating the operating principle of the PDPA system is shown in Figure 2.4.

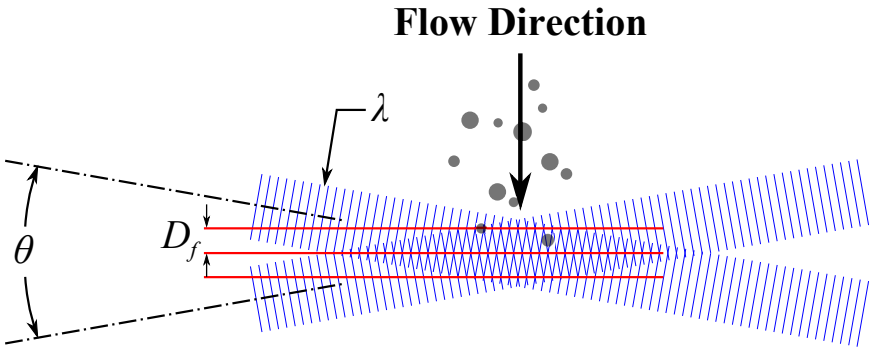

Figure 2.4: PDPA Operating Principle

These lasers intersect at the probe volume where the measurements are made. The PDPA receiver is mounted and aligned so that as a particle passes through the measurement volume, an interference pattern is created at the receiver optics. The doppler burst fequency, known as the Doppler frequency, f_D is related to the particle velocity, U. Here, λ represents the leaser wavelength, θ represents the angle of the intersecting beams, and D_f is the fringe spacing of the interference pattern.

$$U = \frac{\lambda f_D}{2\sin(\theta/2)} \tag{2.1}$$

A four beam system (two lasers with each beam split), is capable of measureing two normal componenets of velocity.

The PDPA system also allows for the measurement of droplet diameters, provided that the droplets are spherical. The PDPA receiver contains 3 optical receivers. The light incident on each receiver travels a different path through the droplet to the receiver, resulting in a phase shift in the Doppler burst. The particle diameter can be found using the phase difference between the signals from two detectors, Φ, the angle between the emitter and receiver, ϕ, the angle of the detectors to the measurement volume, ψ, and the relative index of refraction of the droplets and medium, $n_{\text{rel}} = n_{\text{droplet}}/n_{\text{medium}}$.

$$\Phi = \frac{-2\pi D_p}{\lambda} \frac{n_{\text{rel}} \sin\theta \sin\psi}{\sqrt{2(1+\cos\theta\cos\psi\cos\phi)(1+n_{\text{rel}}^2 - n_{\text{rel}}\sqrt{2(1+\cos\theta\cos\psi\cos\phi)})}} \tag{2.2}$$

2.2 Methodology

In order to generate a flashing spray and obtain the desired measurements, the experiment was assembled and prepared for measurements. First, liquid water was placed within the

hydraulic cylinder. Using a compressed N_2 bottle, the liquid water in the hydraulic cylinder was pressurized to the desired value. This pressure was achieved using a standard pressure regulator. The pressurized liquid water was then heated using the band heaters on the hydraulic cylinder. At the same time, the nozzle assembly was pre-heated to the desired value using the 120 W flexible band heater. The temperature of the nozzle assembly was monitored using the surface mounted thermocouples and the heat supplied was controlled using a variable AC power supply.

While the pressurized water was heating, the PDPA laser system was powered up and allowed to stabilize. The PDPA laser alignment was periodically tested using a PIN diode in order to assure the power achieved was maximized. This was done by adjusting the four degree of freedom fibre launchers and maximizing the output as measured by the PIN diode.. Furthermore ore, the alignment of the PDPA receiver was tested regularly in order to assure the data rates achieved were maximized.

Once the reservoir and nozzle temperatures reached the desired value, the flashing release was initiated by opening the ball valve in the nozzle assembly. The PDPA system recorded data at each radial position until 5000 data points had been collected. The three axis motorized traverse was used in order top collect data at numerous radial positions. Due to the limited time of the flashing release, measurements at a maximum of ten positions were collected.

Data collection was done using the Dantec BSA flow software. The data were collected and sorted according to the operating conditions of the jet. Using multiple measurements at each condition, data averages for each conditions were calculated and tabulated. This allowed for the easy plotting of average values across the radial profile.

In order to properly measure and present the data gathered, the PDPA settings were selected in order to optimize the data rate within the range of values expected. This was done by selecting the operating parameters of the PDPA system. The PDPA settings used were as outlined in the experimental setup chapter and are summarized in Table 2.1.

The PDPA settings were chosen in such a manner as to maximize signal strength while maintaining measurement integrity. The emitter and receiver focal length were selected from a variety of possible options. A small emitter focal length results in a smaller probe volume with higher power density, thereby providing improved signal strength, particularly in dense sprays. However, as the emitter focal length is decreased, the maximum measurable diameter is reduced. Based on the manufacturer's specifications, the maximum measurable diameter was chosen to be approximately 10 times the largest expected diameter. This

Table 2.1: PDPA Settings and Parameters

Property		Value
Laser Power (nominal)	Nd:YAG	25 mW
	HeNe	20 mW
Laser Wavelength	Nd:YAG	532 nm
	HeNe	632.8 nm
Emitter Focal Length		400 mm
Receiver Focal Length		310 mm
Velocity Range		$0 - 50$ m/s
Diameter Range		$0 - 200$ μm

allowed for accurate measurements and provided some allowance for particles larger than expected. The velocity range was chosen in the Dantec software and the range was centered about the typical mean centerline velocity.

The PDPA software collected the data and performed some initial post processing of them. Further post processing for this study was performed using customs scripts in commercial software(MATLAB 2012a). The data sets gathered include 5000 data points at each measurement location. The collection of 5000 data points was chosen as a compromise between limiting uncertainty in the data and collection time. Given the limited volume of fluid available in each flashing release, the time available for measurements was limited to approximately 90 s. Li *et al.* (2012) state that for an accuracy of 5% with a 95% confidence interval, a minimum of 5000 individual diameter measurements is needed. With 5000 data points at each location, typical 95% confidence intervals in measurements of D_{32} were $\pm 0.1 - 0.2\,\mu$m for each measurement.

Another important parameter of the flash atomization system was the nozzle. The nozzle used was a conical converging-diverging nozzle as illustrated in Figure 2.5. Nozzle dimensions are summarized in Table 2.2. If the flow rate of the nozzle was too high, the large amount of light attenuation through the spray resulted in limited or negligible data rates from the PDPA system. As such, several nozzles with different throat diameters were built and tested in order to achieve an acceptable flow rate while still preserving the ability to utilize the PDPA system. It was found that a throat diameter of 0.8 mm proved an acceptable option. Based on the outlet diameter of $D_2 = 1.6$ mm, the chosen nozzle has an aspect ratio of $L/D \approx 16$.

The diameter distributions collected are presented in this paper on a logarithmic scale

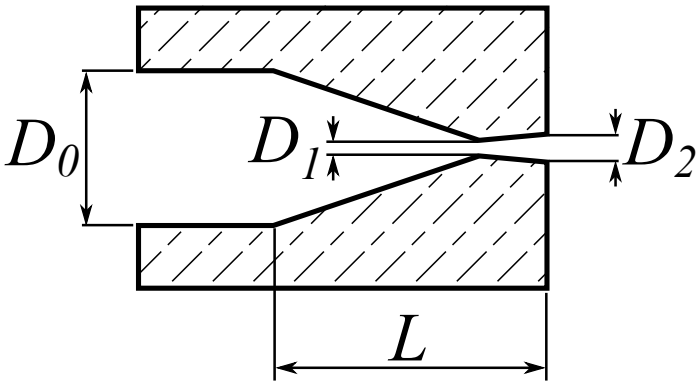

Figure 2.5: Nozzle geometry

Table 2.2: Nozzle dimensions

Dimension	D_0	D_1	D_2	L
Value (mm)	10.3	0.8	1.6	25.4

since droplet size distributions typically follow a log-normal distribution(Bowen (2012)). This presentation is done by using logarithmically scaled diameter bins for the construction and presentation of the probability distribution functions. In presenting the data in this manner, the characteristics of the distribution at small diameters is not obscured by the relatively large span of the data set. Figure 2.6 represents a characteristic diameter distribution with linear axes whereas Figure 2.7 illustrates the same distribution on a logarithmic axis. From these figures, it is clear that the use of linear axes obscures the characteristics of the distribution, particularly at small diameters.

A final set of experiments was performed with the purpose of collecting long exposure photographs of the spray. This was done in order to observe the effects of the inlet conditions on the spray in aggregate. While the PDPA system provides detailed and concurrent measurements of both velocity and diameter, the measurement is confined to one spatial position of the probe volume. The use of long exposure photography, while unable to provide either velocity nor diameter measurements, illustrates the effect of inlet conditions on the angle of the spray. In order to obtain these measurements, back scatter images were collected over the course of a 30 s exposure. This method minimizes the effect of instantaneous instabilities in the spray while maximizing the contrast in the image. A calibration image was collected in order to provide a scale for the images. The spreading angle of the spray was characterized using two measurements. The near-field spreading angle, θ_n was measured in the region of $z = 3.4 - 10.2$ mm and the far-field spreading angle was measured

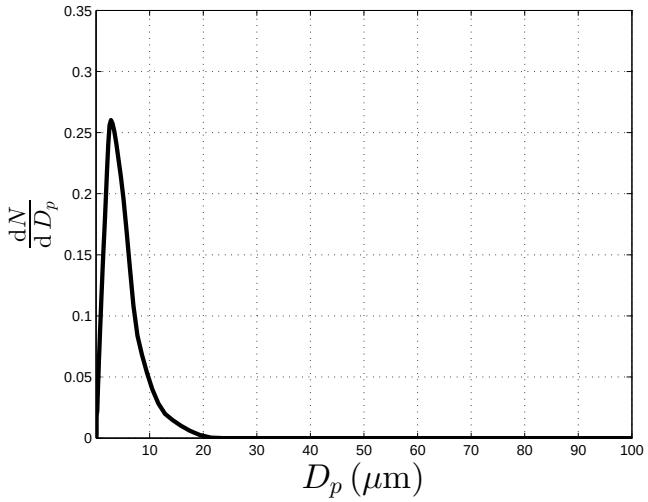

Figure 2.6: Probability density function with linear abscissa

in the region of $z = 45.0 - 190\,\mathrm{mm}$. The angles were measured using binarized images in order to locate the edge of the spray. The process of the edge detection is outlined in Figure 2.8.

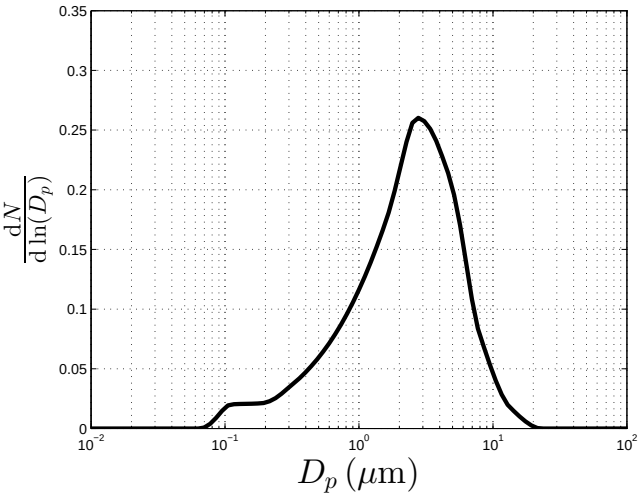

Figure 2.7: Probability density function with logarithmic abscissa

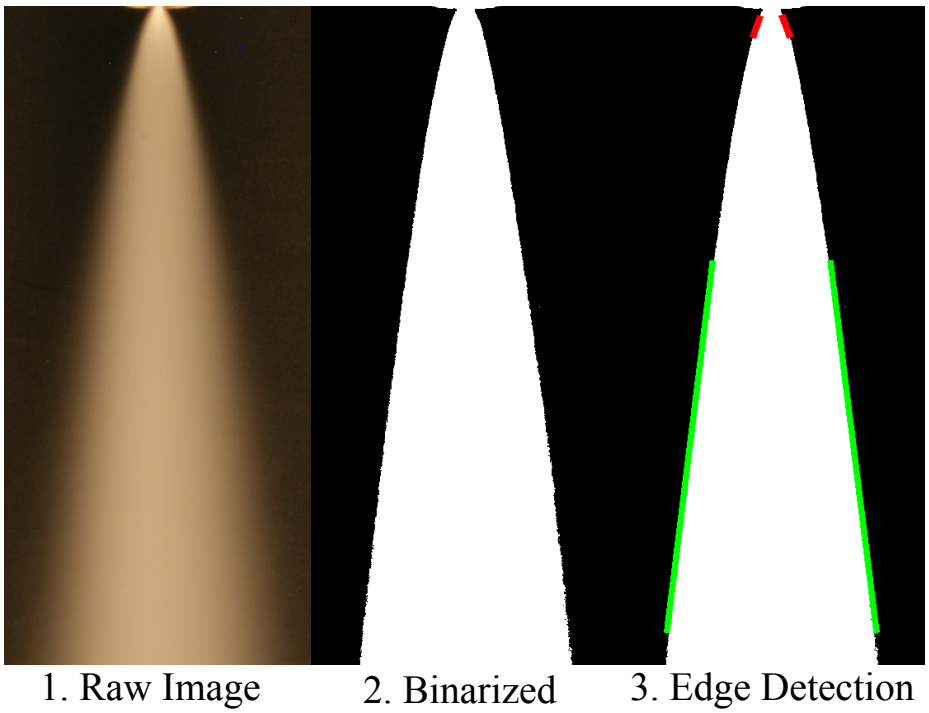

Figure 2.8: Process of detecting spray edges for spreading angle measurement

Chapter 3

Experimental Results

3.1 Velocity Measurements

3.1.1 Radial Profiles of Droplet Velocity

The PDPA system was used in order to concurrently measure the droplet velocity and diameter. By using the three axis traverse system, the measurements were made across the spray profile. The velocity profiles represent the average droplet velocity, U_z at various radial locations for an axial location of $z = 150\,\text{mm}$. The measurements were made from the jet centerline towards the jet periphery. Due to declining data rates near the periphery of the spray, PDPA measurements could not be collected beyond $r = 30\,\text{mm}$. Beyond this point, the low droplet velocity and low spray density resulted in prohibitively low data rates.

Figures 3.1 through 3.4 represent the effect of the reservoir pressure on the velocity profiles of the spray. Each individual figure represents data collected at a single reservoir temperature, but at a variety of pressures. This allows for the observation of the effect of changing reservoir pressure has on the droplet velocity profile for a given reservoir temperature.

These data were also used to produce plots demonstrating the effect of reservoir temperature on the droplet velocity profile. Figures 3.5 through 3.8 represent the droplet velocity profiles collected at constant reservoir pressures. In doing so, each individual figure illustrates the effect of reservoir temperature on the droplet velocity profile.

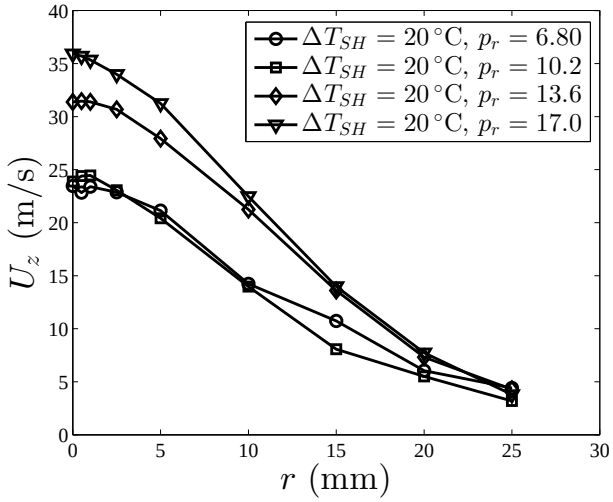

Figure 3.1: Radial profile of U_z with $\Delta T_{SH} = 20\,^{\circ}\mathrm{C}$

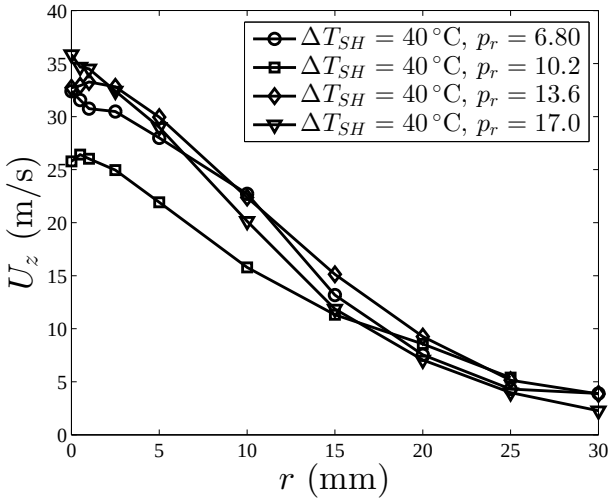

Figure 3.2: Radial profile of U_z with $\Delta T_{SH} = 40\,^{\circ}\mathrm{C}$

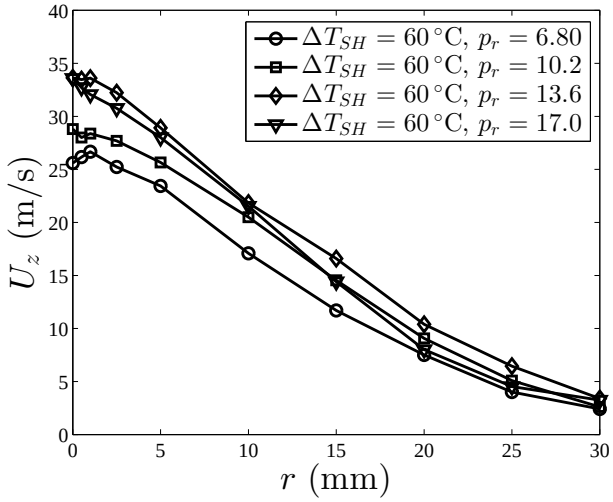

Figure 3.3: Radial profile of U_z with $\Delta T_{SH} = 60\,^{\circ}\mathrm{C}$

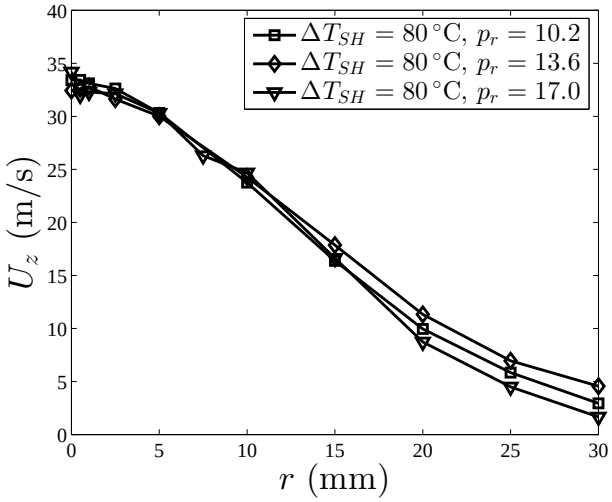

Figure 3.4: Radial profile of U_z with $\Delta T_{SH} = 80\,^{\circ}\mathrm{C}$

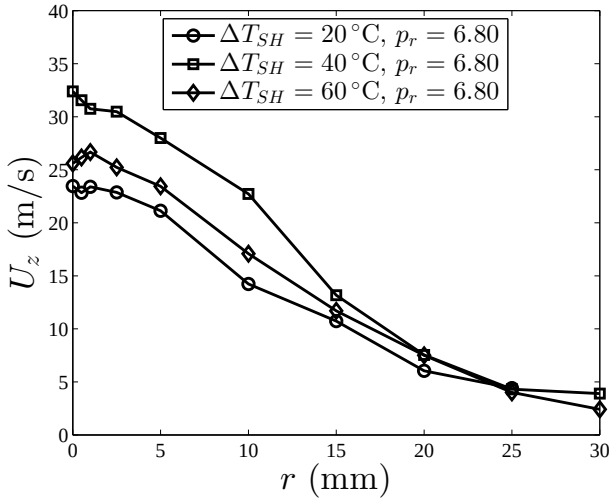

Figure 3.5: Radial profile of U_z with $p_r = 6.8$

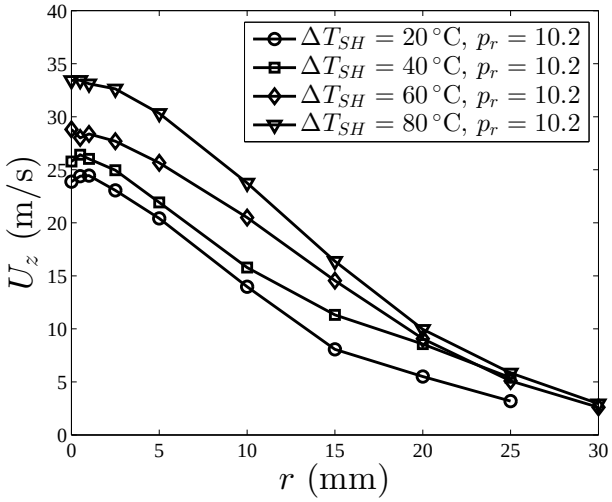

Figure 3.6: Radial profile of U_z with $p_r = 10.2$

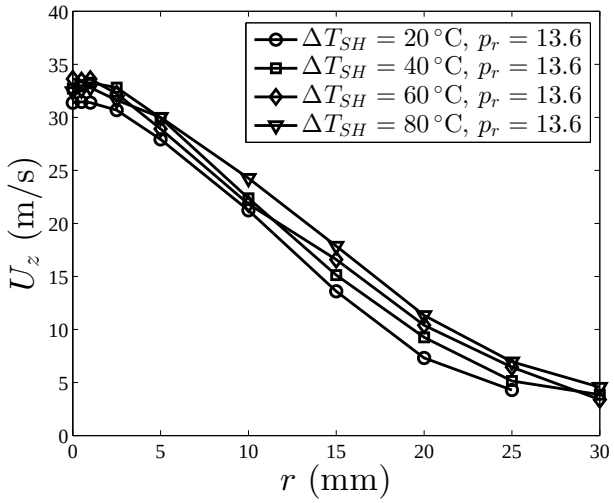

Figure 3.7: Radial profile of U_z with $p_r = 13.6$

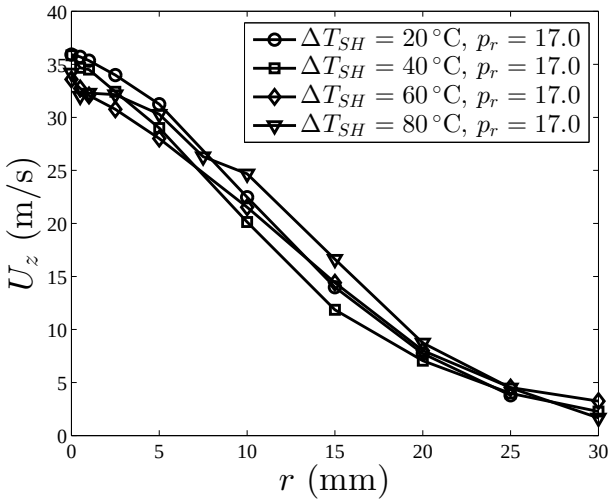

Figure 3.8: Radial profile of U_z with $p_r = 17.0$

3.1.2 Velocity Plots

The profile plots included earlier provide insight into the effect of the reservoir conditions on the overall velocity profiles. However, it can be difficult to observe local trends in the data. In order to more accurately depict the effect of reservoir conditions on localized droplet velocities, the localized effects of upstream conditions were plotted. These figures represent the effect of varying a single upstream condition (p_r or ΔT_{SH}) on the droplet velocities measured at a single radial position.

Figures 3.9 through 3.12 represent the effect of the pressure ratio on the measured values of U_z at various radial locations. Each of set of figures contains data collected at a different value of ΔT_{SH}. These figures assist in determining the effect of the inlet conditions on the droplet velocity at a variety of radial locations. The evolution of these relations as the radial position is increased can also be observed. The droplet velocities at various radial positions were also plotted as a function of the degree of super-heat. These plots are presented in Figures 3.13 through 3.16.

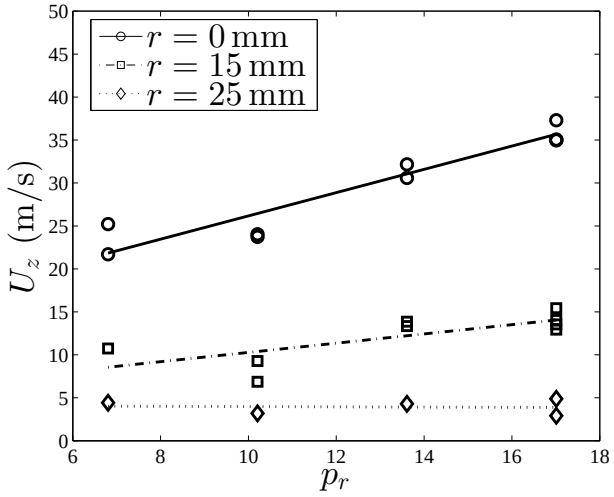

Figure 3.9: Effect of p_r on U_z at various radial locations with $\Delta T_{SH} = 20\,^{\circ}\mathrm{C}$

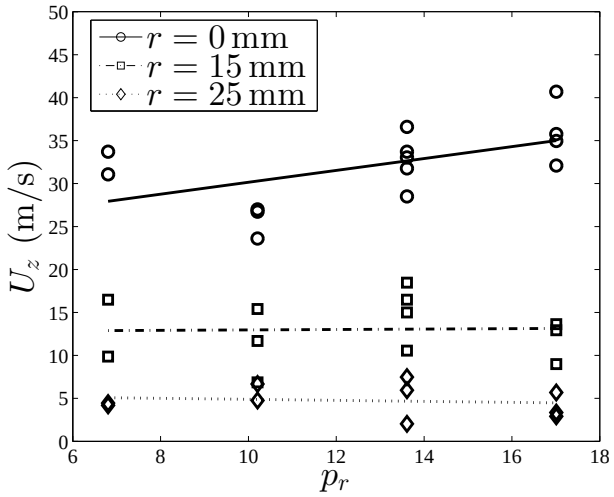

Figure 3.10: Effect of p_r on U_z at various radial locations with $\Delta T_{SH} = 40\,^{\circ}\mathrm{C}$

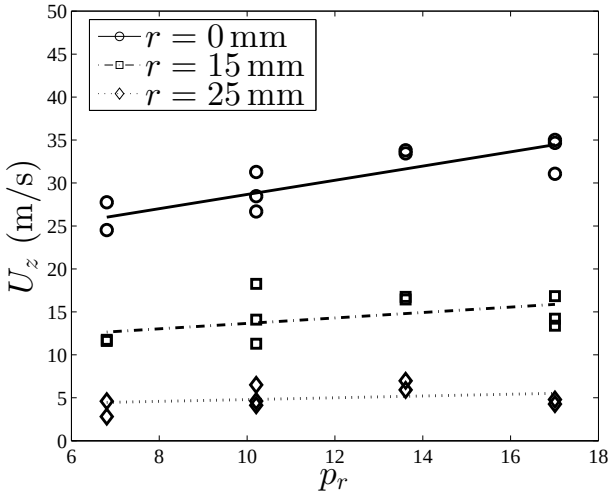

Figure 3.11: Effect of p_r on U_z at various radial locations with $\Delta T_{SH} = 60\,^{\circ}\mathrm{C}$

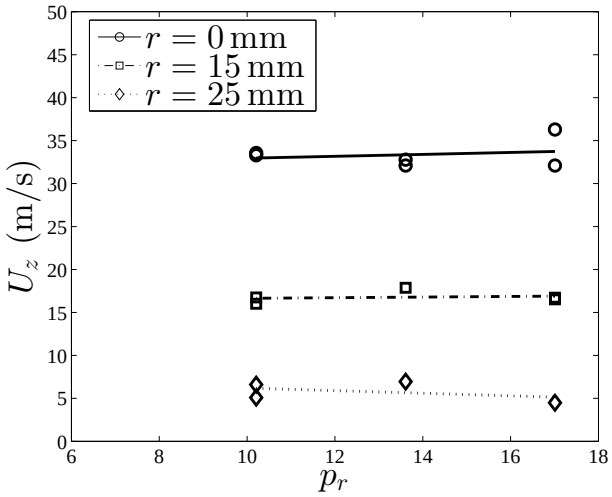

Figure 3.12: Effect of p_r on U_z at various radial locations with $\Delta T_{SH} = 80\,^{\circ}\mathrm{C}$

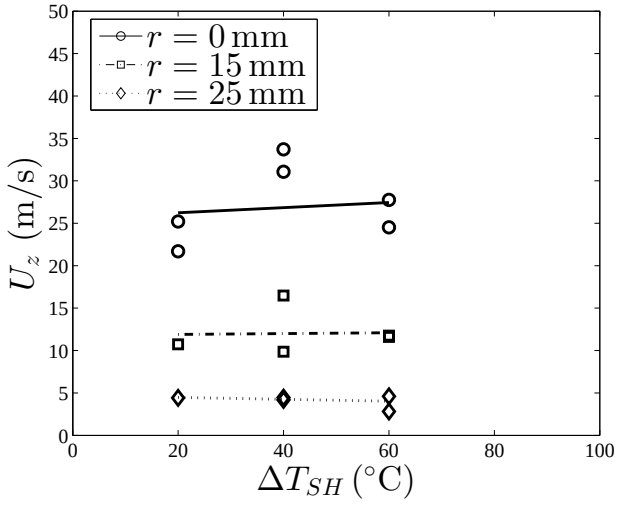

Figure 3.13: Effect of ΔT_{SH} on U_z at various radial locations with $p_r = 6.80$

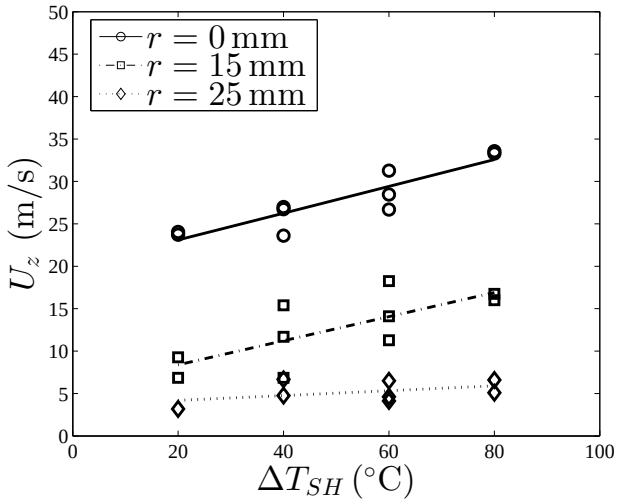

Figure 3.14: Effect of ΔT_{SH} on U_z at various radial locations with $p_r = 10.2$

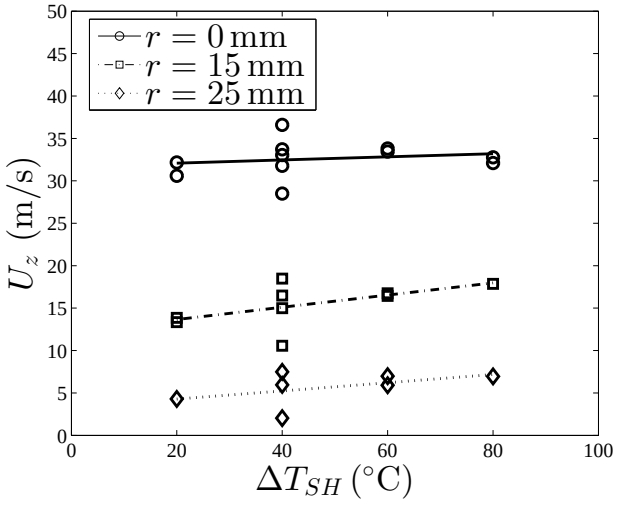

Figure 3.15: Effect of ΔT_{SH} on U_z at various radial locations with $p_r = 13.6$

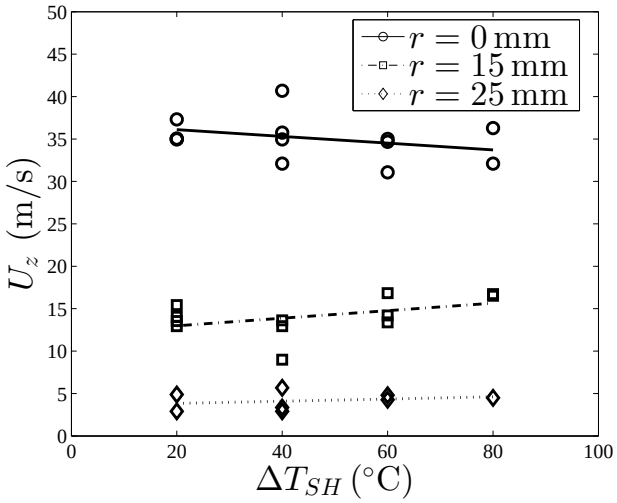

Figure 3.16: Effect of ΔT_{SH} on U_z at various radial locations with $p_r = 17.0$

3.2 Long Exposure Images

In order to independently determine the qualitative effect of reservoir temperature and reservoir pressure on the spray envelope, a series of long exposure photographs of the spray was taken. The spray was tested under a variety of operating conditions and for each condition tested, a 30 second exposure photograph was taken. These images were used in order to determine the effects of p_r and ΔT_{SH} on both the spreading angle as well as the operating regime of the spray.

Figure 3.17 represents the effect of reservoir pressure on the spray envelope. This figure includes photographs at 4 reservoir pressures. In each case, the degree of superheat was maintained at $\Delta T_{SH} = 60\,^{\circ}\mathrm{C}$. This figure allows for the determination of the effect of the pressure ratio on the spray angle and envelope of the spray operating at a constant degree of superheat.

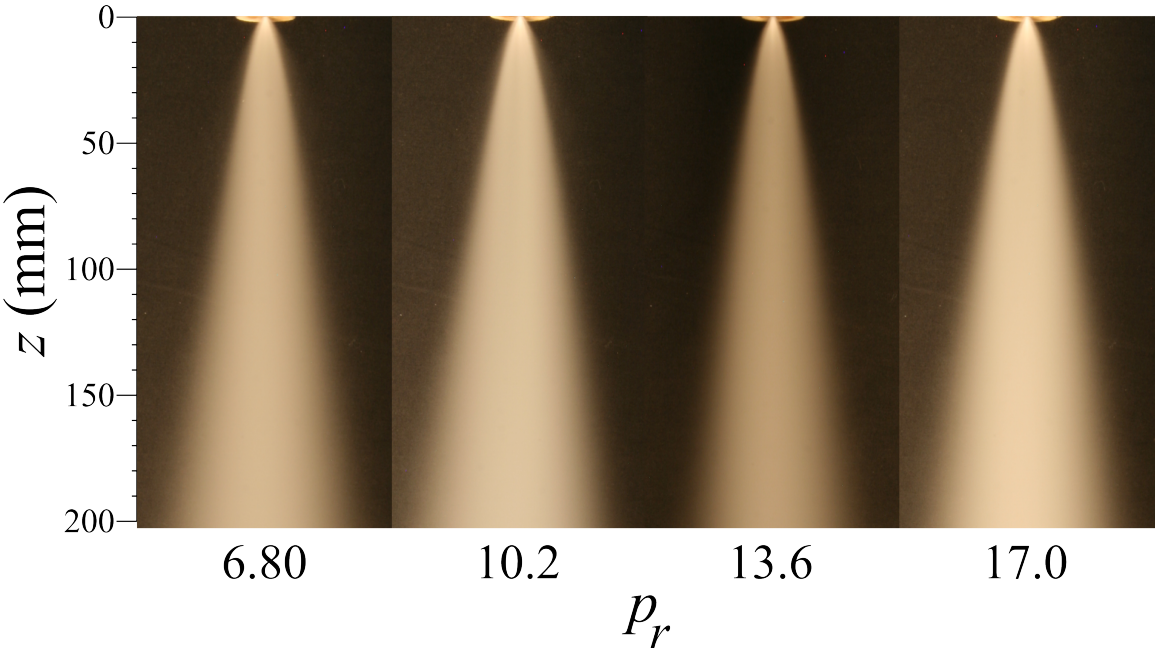

Figure 3.17: The effect of p_r on a flash atomized spray
All measurements made with $\Delta T_{SH} = 60\,^{\circ}\mathrm{C}$

This figure shows no discernable qualitative difference in the spray operating at the various pressure ratios tested. In each case, the spreading angle appears approximately equal and the spray regime appears constant.

Figure 3.18 represents the effect of reservoir pressure on the spray envelope. This figure includes photographs at 4 reservoir pressures. In each case, the pressure ratio was maintained at $p_r = 10.2$. This figure allows for the determination of the effect of the degree of

superheat on the spray angle.

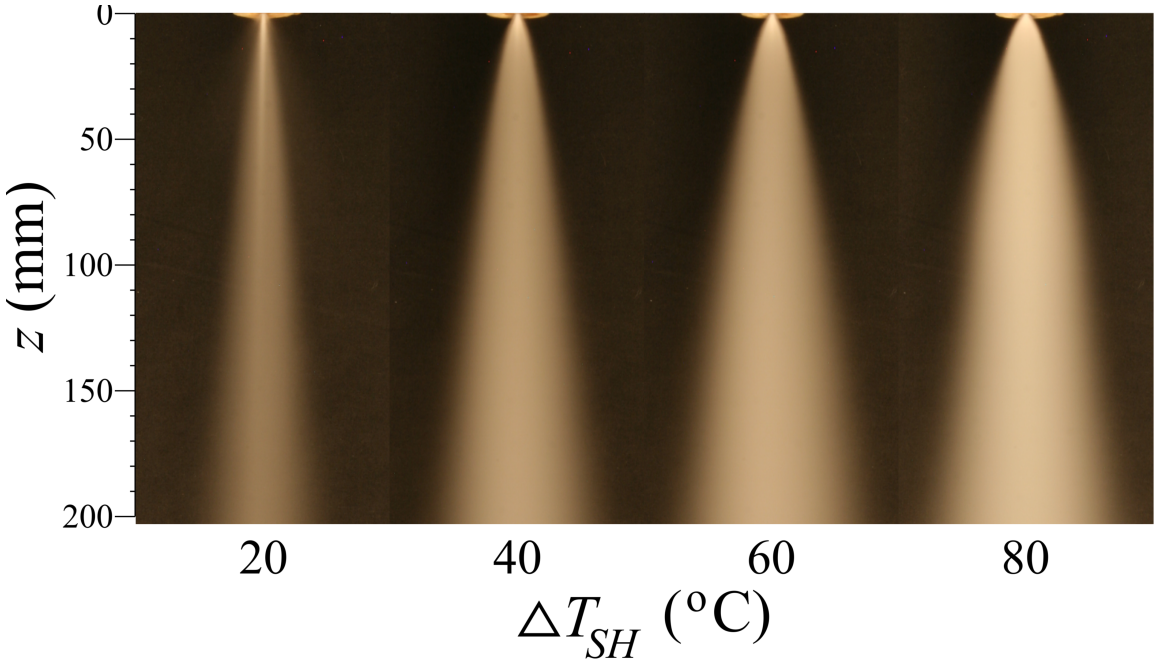

Figure 3.18: The effect of ΔT_{SH} on a flash atomized spray
All measurements made with $p_r = 10.2$

In this figure, a clear effect of the degree of superheat on the spray characteristics is apparent. At low degrees of superheat, the spray is relatively narrow and there appears to exist an intact liquid core. As the degree of superheat is increased, the spray angle increases and the spray regime appears more uniform.

A quantitative analysis on the spray angle under various operating conditions was performed. The long exposure photographs were binarized in software and the near-field spreading angle, θ_n and the far-field spreading angle θ_f were measured using an edge detection algorithm. The results obtained were plotted as functions of ΔT_{SH} and p_r, and are shown in Figures 3.19 and 3.20, respectively.

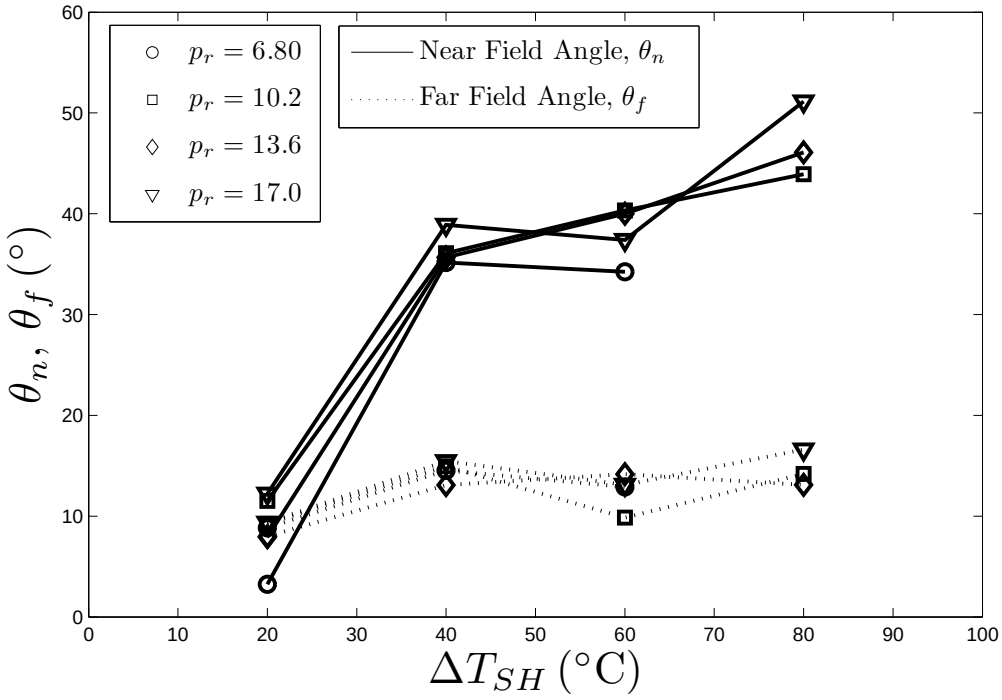

Figure 3.19: Effect of ΔT_{SH} on θ_n and θ_f.

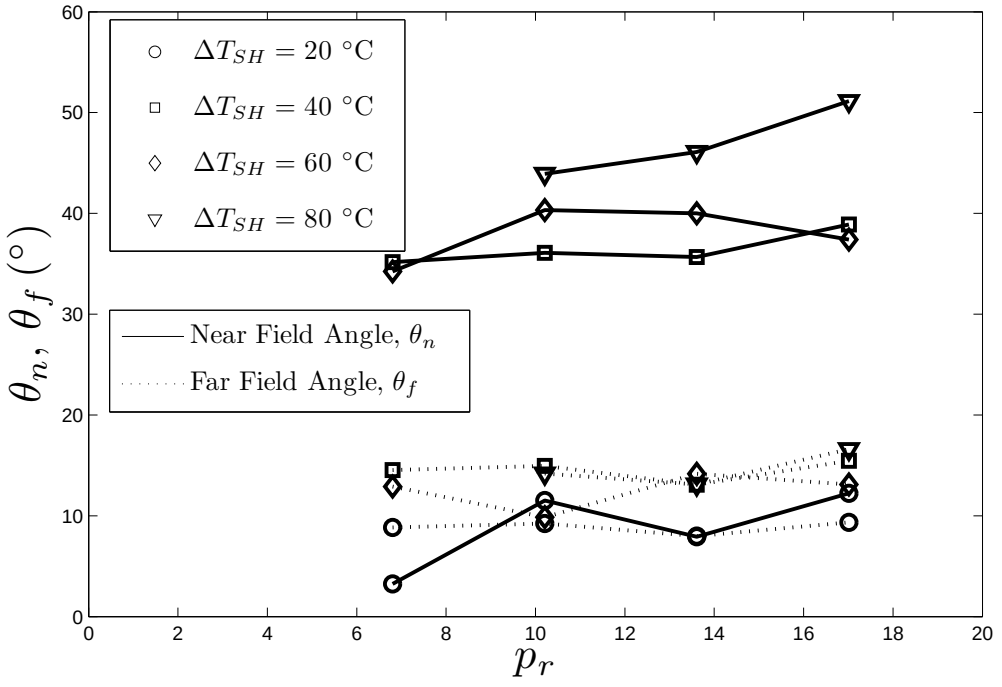

Figure 3.20: Effect of p_r on θ_n and θ_f.

3.3 Data Rate Profiles

The long exposure photographs provide some measure of the width of the spray envelope. However, because the width of the spray envelope in the binarized images is dependent on the image processing technique, these images provide only qualitative results. The normalized data rate, $\bar{N}$, of the PDPA system provides some insight into the droplet density of the spray. $\bar{N}$ represents the frequency of measurement events recorded by the PDPA. This value is normalized to the maximum data rate in each radial profile in order to allow for comparison of relative values under various operating conditions. This is not a predictive measure, however, because the PDPA system does not perform ideally when the measurement volume occupies a highly dense region of the spray, or in regions containing large numbers of non-spherical liquid ligaments. Regardless, the radial profile of the PDPA data rate provides a measure of the spray density, particularly in regions where the measurement volume is not obscured.

Figures 3.21 through 3.24 show the radial profiles of the PDPA data rate at various degrees of superheat and a pressure ratio of 13.6. The values of the data rate are normalized to the maximum data rate at each condition. This allows for the comparison of the relative data rates at various operating conditions.

Figures 3.25 through 3.28 help demonstrate the effect of the degree of superheat in the radial profiles of the normalized data rate. These figures show the radial profile of the PDPA data rate as temperature was varied at a constant pressure ratio of 17.0. Again, these figures are normalized to the local maximum data rate in order to facilitate the comparison between the figures.

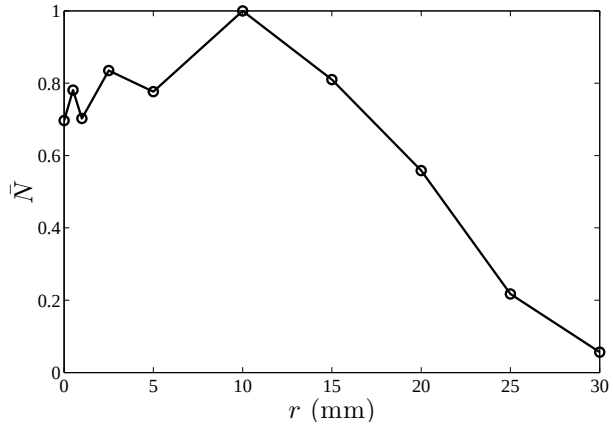

Figure 3.21: Radial profile of $\bar{N}$ with $p_r = 6.8$ and $\Delta T_{SH} = 60\,^{\circ}\mathrm{C}$

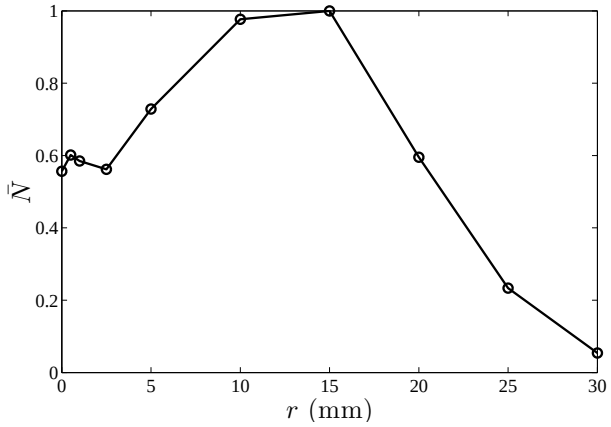

Figure 3.22: Radial profile of $\bar{N}$ with $p_r = 10.2$ and $\Delta T_{SH} = 60\,^{\circ}\mathrm{C}$

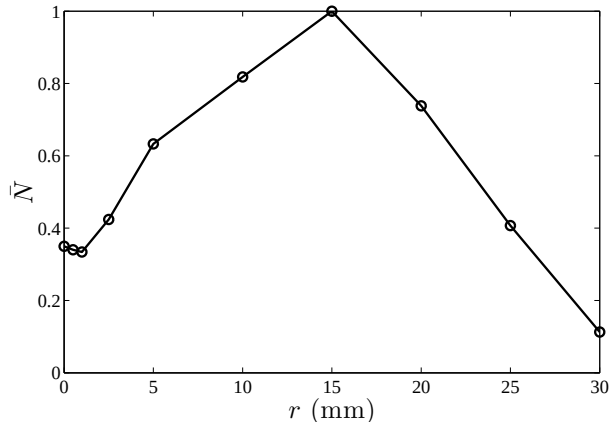

Figure 3.23: Radial profile of $\bar{N}$ with $p_r = 13.6$ and $\Delta T_{SH} = 60\,^{\circ}\mathrm{C}$

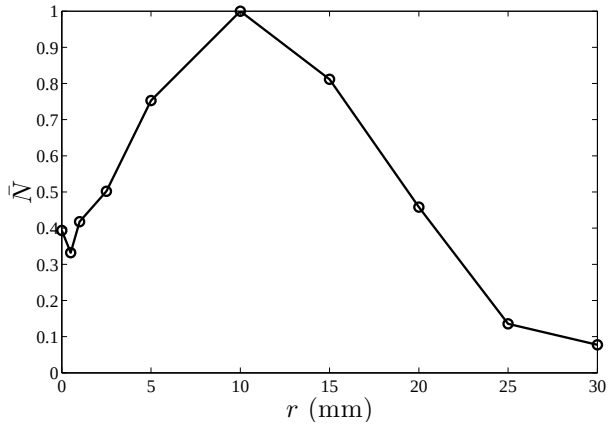

Figure 3.24: Radial profile of $\bar{N}$ with $p_r = 17.0$ and $\Delta T_{SH} = 60\,^{\circ}\mathrm{C}$

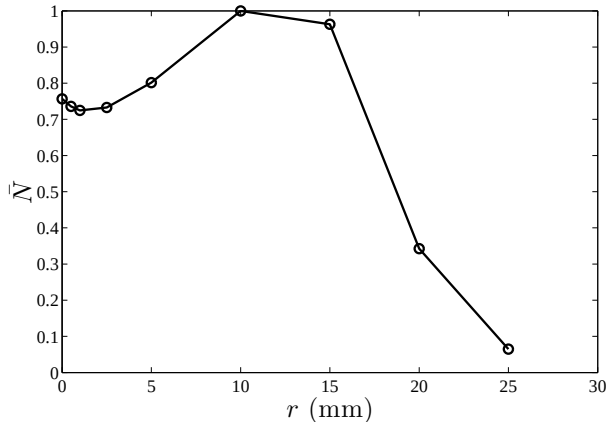

Figure 3.25: Radial profile of $\bar{N}$ with $p_r = 17.0$ and $\Delta T_{SH} = 20\,^{\circ}\mathrm{C}$

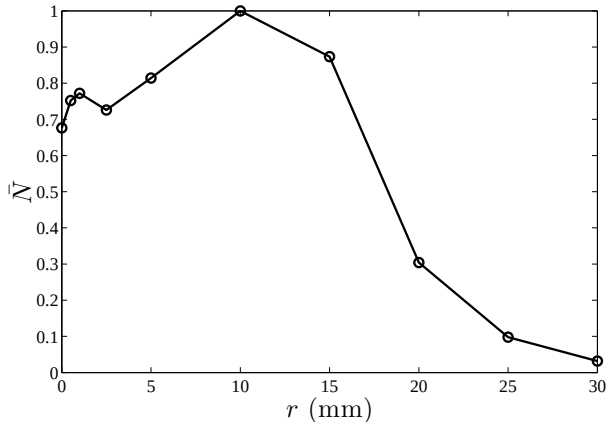

Figure 3.26: Radial profile of $\bar{N}$ with $p_r = 17.0$ and $\Delta T_{SH} = 40\,^{\circ}\mathrm{C}$

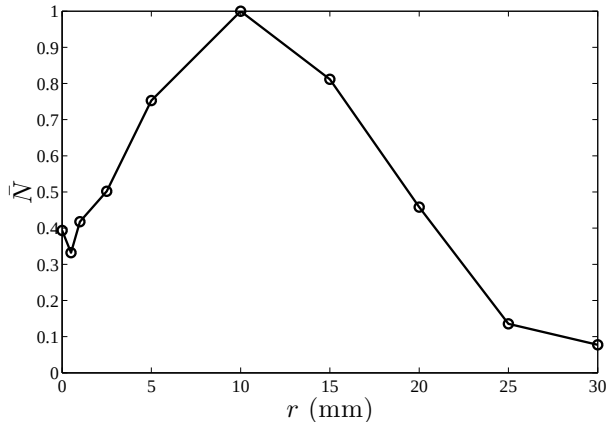

Figure 3.27: Radial profile of $\bar{N}$ with $p_r = 17.0$ and $\Delta T_{SH} = 60\,^{\circ}\mathrm{C}$

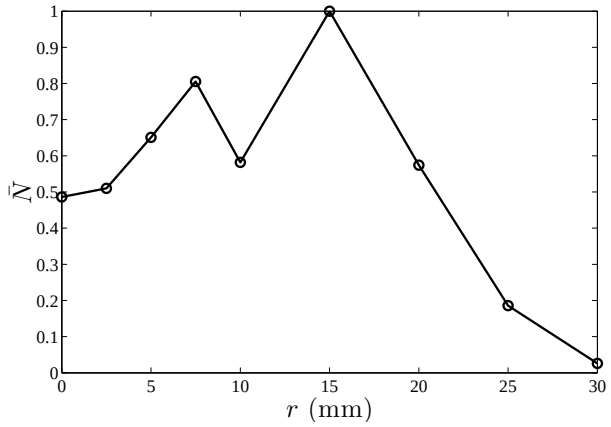

Figure 3.28: Radial profile of $\bar{N}$ with $p_r = 17.0$ and $\Delta T_{SH} = 80\,^{\circ}\mathrm{C}$

3.4 Diameter Measurements

The droplet distribution is a vitally important characteristic of an atomized spray. Droplet diameter influences the combustion characteristics of fuel sprays and the measurement of droplet size in flash atomized sprays is an active area of research. Concurrent with the velocity measurements, droplet diameters were also measured with the PDPA system.

3.4.1 Diameter Profiles

Using the PDPA system and the three axis traverse, the average droplet diameters across the radial profile of the spray at an axial distance of $z = 150\,\text{mm}$ were measured. These measurements were performed at a variety of pressures and temperatures and are illustrated in Figures 3.29 through 3.32. These measurements allow for the determination of the spatial distribution of the droplets based on the droplet diameter. Each figure presented represents a series of tests at varying temperature with a constant reservoir pressure. The scale of the D_{32} axis is kept constant in each figure in order to more easily compare the trends observed in each figure. These results are presented, as is the standard in spray research, using the Sauter mean diameter, D_{32} as a measure of the droplet size. The use of D_{32} provides a measure of the volume to surface area ratio, and is a particularly useful measure in the field of reactive flows. The Sauter mean diameter is defined as follows:

$$D_{32} = \frac{\sum D_p^3}{\sum D_p^2} \tag{3.1}$$

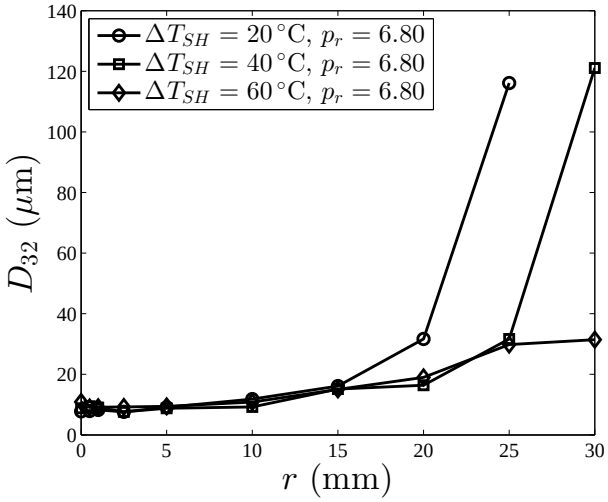

Figure 3.29: Radial profile of D_{32} with $p_r = 0.6.8$

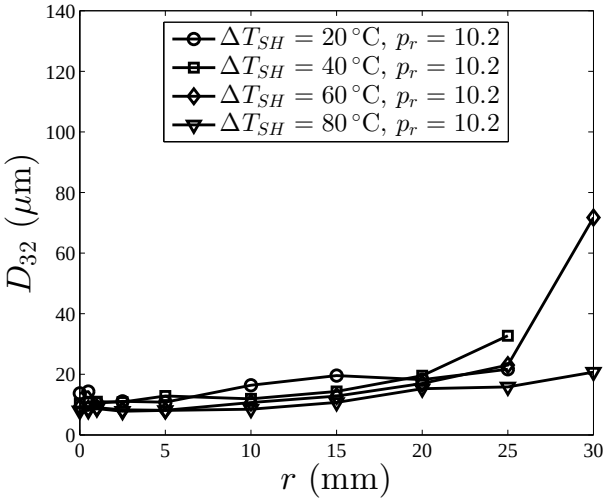

Figure 3.30: Radial profile of D_{32} with $p_r = 10.2$

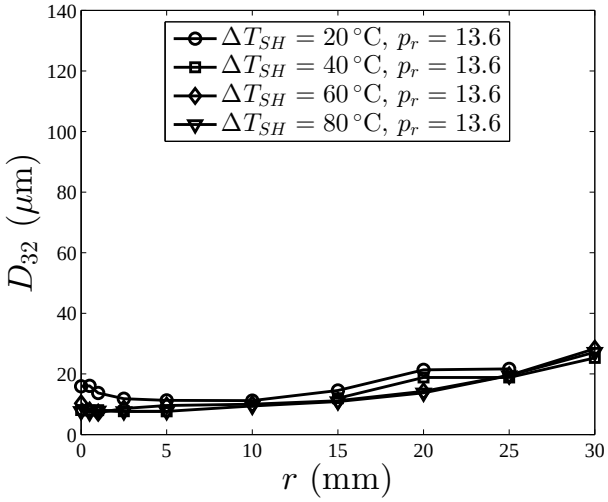

Figure 3.31: Radial profile of D_{32} with $p_r = 13.6$

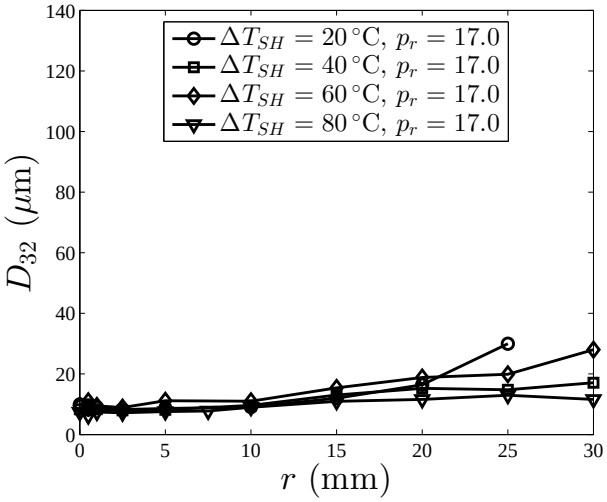

Figure 3.32: Radial profile of D_{32} with $p_r = 17.0$

With the figures presented as they were, with equal scaling of the D_{32} axis, the differences between figures is made clear. However, in doing this, the variations within each individual figure are not always obvious. As such, the same figures are reproduced in Figures 3.33 through 3.36, with each axis scaled to the view the centerline values. This allows for the observation of local trends, particularly at higher pressures where the centerline to peripheral variance in D_{32} is relatively small.

Using the same data, the figures can be presented in another manner. Figures 3.37 through 3.40 illustrate the same profiles of D_{32}. However, in these figures, the data are presented such that each figure contains test data at various reservoir pressures but with constant temperatures. In this manner, the effect of changing reservoir temperatures on the profile of D_{32} can more easily be determined.

Again, a similar trend is observed. With $\Delta T_{SH} = 20\,^{\circ}\mathrm{C}$ there is a large variation between the centerline and peripheral values of D_{32}. At $\Delta T_{SH} = 80\,^{\circ}\mathrm{C}$, this variation is lessened, resulting again in a more uniform atomization. At higher reservoir temperatures, the scatter of values at all radial positions appears to decrease. This indicates that at high temperatures, the atomization is consistent and demonstrates some robustness with regards to changes in reservoir pressure.

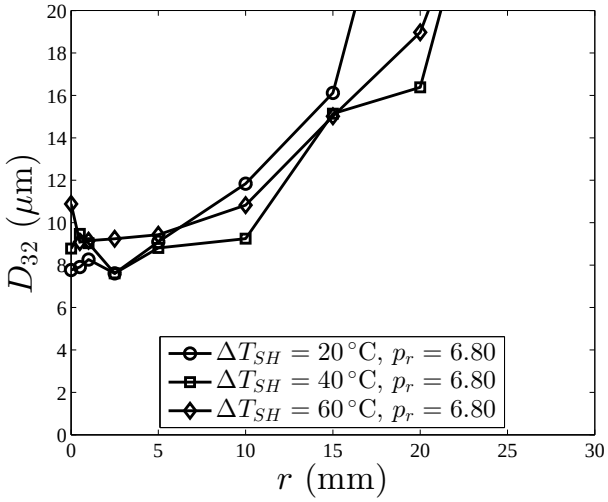

Figure 3.33: Radial profile of D_{32} with $p_r = 6.8$ with scaled axis.

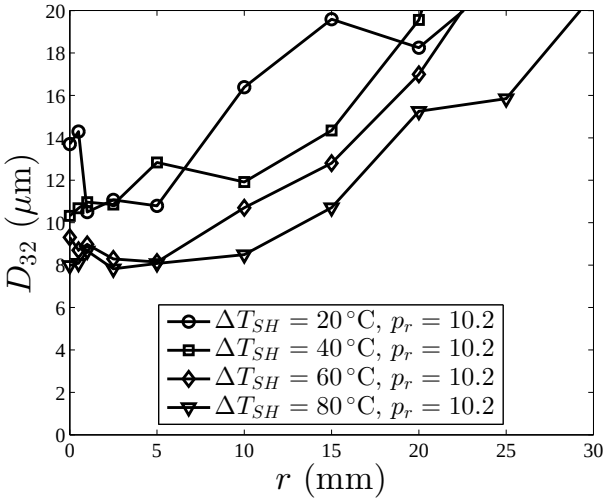

Figure 3.34: Radial profile of D_{32} with $p_r = 10.2$ with scaled axis.

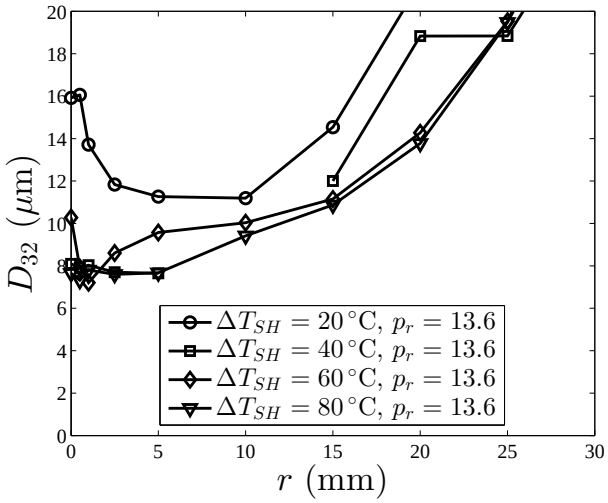

Figure 3.35: Radial profile of D_{32} with $p_r = 13.6$ with scaled axis.

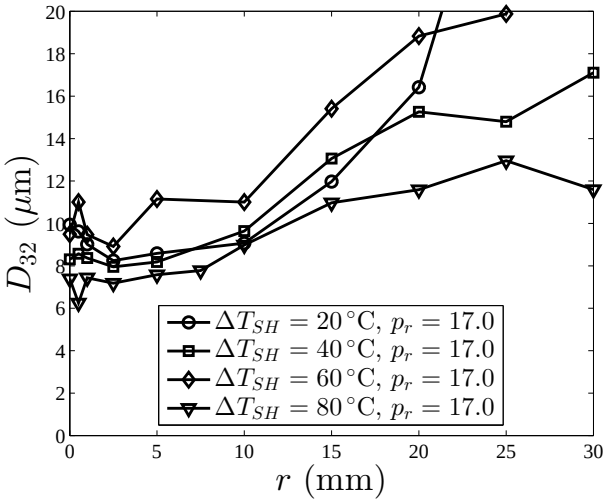

Figure 3.36: Radial profile of D_{32} with $p_r = 17.0$ with scaled axis.

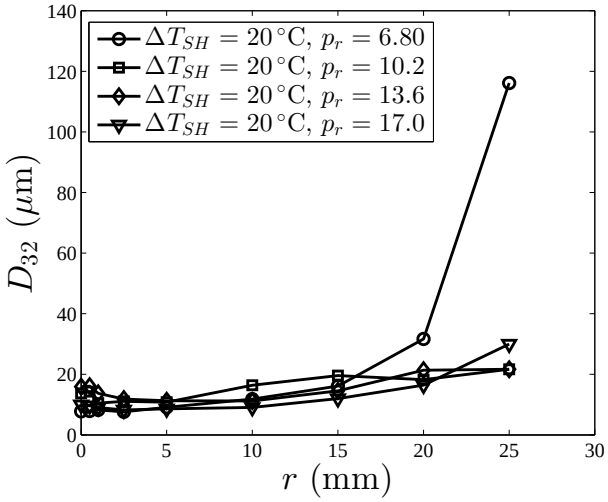

Figure 3.37: Radial profile of D_{32} with $\Delta T_{SH} = 20\,^{\circ}\mathrm{C}$

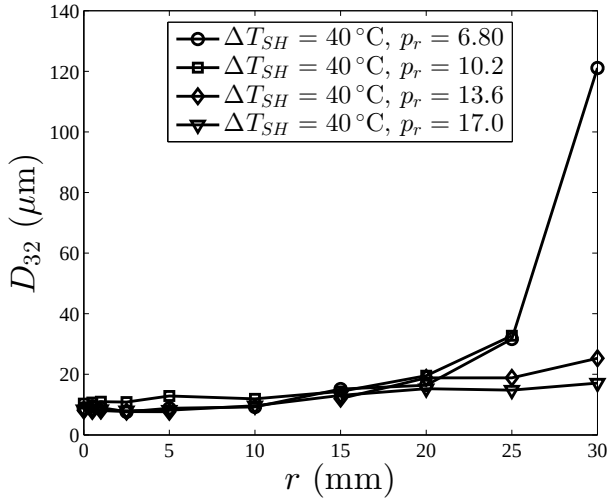

Figure 3.38: Radial profile of D_{32} with $\Delta T_{SH} = 40\,^{\circ}\mathrm{C}$

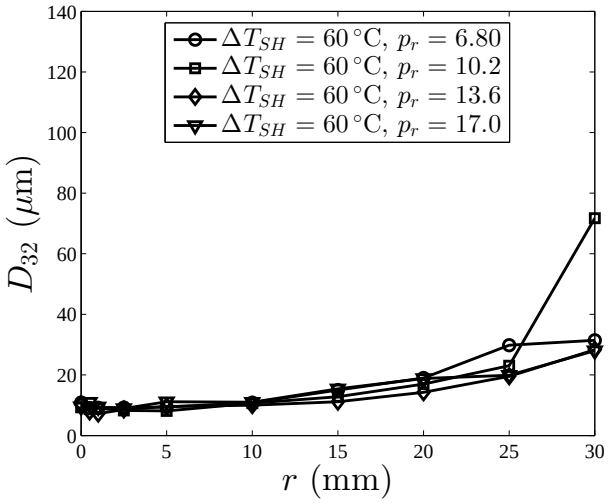

Figure 3.39: Radial profile of D_{32} with $\Delta T_{SH} = 60\,^{\circ}\mathrm{C}$

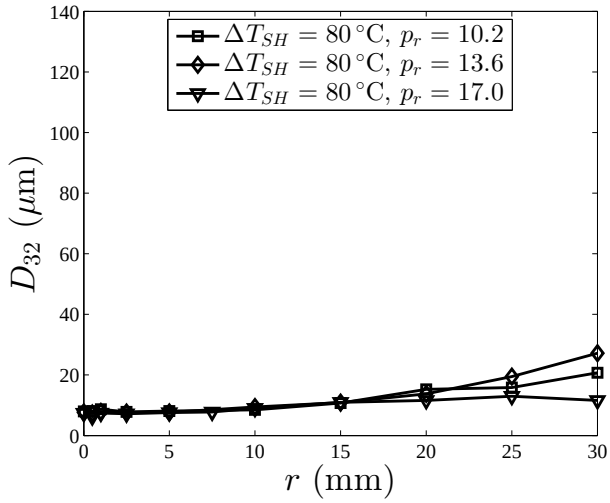

Figure 3.40: Radial profile of D_{32} with $\Delta T_{SH} = 80\,^{\circ}\mathrm{C}$

As with the radial D_{32} profiles plotted at constant pressure, the radial profiles plotted at constant temperature are also reproduced with axes scales such that the variations along the spray centerline are visible. These plots are shown in Figures 3.41 through 3.44.

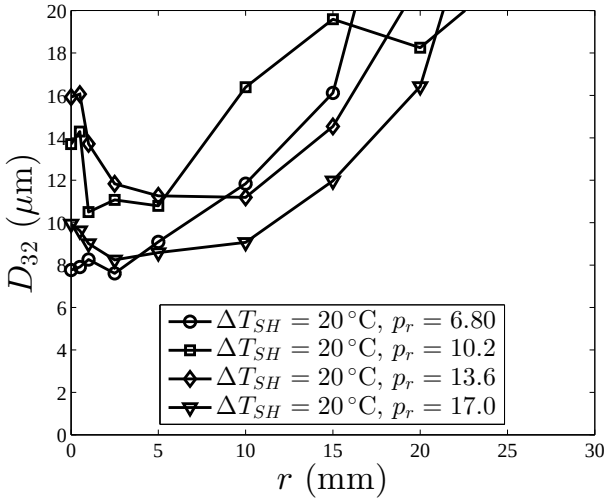

Figure 3.41: Radial profile of D_{32} with $\Delta T_{SH} = 20\,^{\circ}$C with scaled axis.

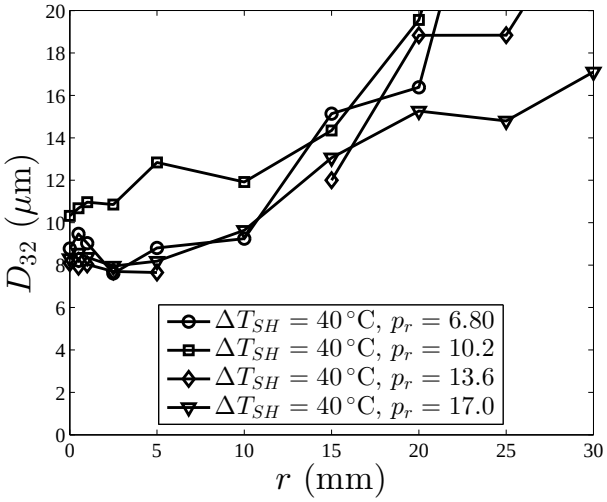

Figure 3.42: Radial profile of D_{32} with $\Delta T_{SH} = 40\,^{\circ}$C with scaled axis.

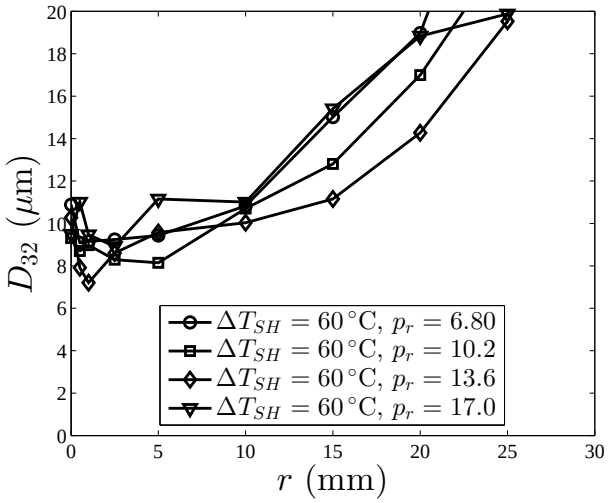

Figure 3.43: Radial profile of D_{32} with $\Delta T_{SH} = 60\,^{\circ}$C with scaled axis.

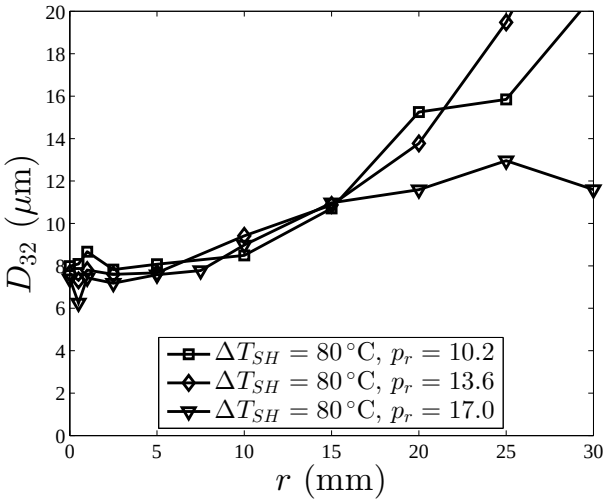

Figure 3.44: Radial profile of D_{32} with $\Delta T_{SH} = 80\,^{\circ}$C with scaled axis.

The centerline values of D_{32} are summarized in Table 3.1. This table lists the centerline D_{32} values at all tested conditions. Also included is an uncertainty estimate in the D_{32} values. This estimate considers both the measurement uncertainty of the PDPA as well as the repeatability uncertainty from the number of repeated trials. This error was determined using student's t-distribution to a confidence level of 95%.

Table 3.1: Centerline D_{32} summary

p_r (−)	ΔT_{SH} (°C)	D_{32} (µm)	$\epsilon_{D_{32}}$ (µm)*
0.68	20	7.8	0.2
	40	8.8	5.6
	60	10.9	3.1
	80	(−)	(−)
10.2	20	13.7	3.7
	40	10.3	2.4
	60	9.3	3.5
	80	8.0	2.3
13.6	20	15.9	4.8
	40	8.1	0.7
	60	10.3	7.0
	80	7.7	1.1
17.0	20	9.3	1.7
	40	8.3	0.7
	60	9.5	1.0
	80	7.9	0.8

*$p = 0.95$ confidence

3.5 Probability Density Functions

While the average droplet diameter is an important quantity, the distribution of droplet diameters at a given location is also a valuable measure. D_{32} is used for the aggregate measure of droplet size, and given its definition in Equation 3.1, the value obtained is more affected by large droplets. As such, the probability density functions (PDFs) of droplet diameters along the jet center line were measured.

Figure 3.45 includes PDFs of the particle diameter, D_p along the jet centerline. In this figure, all measurements were taken with $\Delta T_{SH} = 60\,^{\circ}\mathrm{C}$. The pressure ratio was varied and the PDFs were plotted on a single figure. This was done in order to observe the effect of the pressure ratio on the droplet diameter distribution.

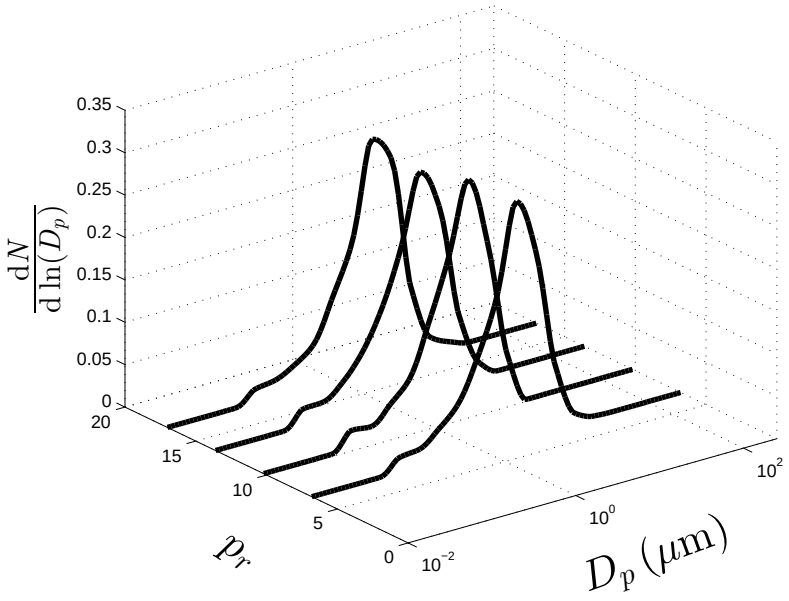

Figure 3.45: Probability functions with $\Delta T_{SH} = 60\,^{\circ}\mathrm{C}$

The PDFs of the droplet diameters were reproduced in order to determine the effect of the degree of superheat on the droplet diameter distribution. In Figure 3.46, the PDFs of the droplets diameters are shown. This figure presents data collected at a constant pressure ratio with a variable degree of superheat.

The values of the particle diameters along the jet centerline at all operating conditions tested are shown in Table 3.2. This table includes the mean, μ_{D_p} and standard deviation, σ_{D_p} of the particle diameters. Also included in this table are the geometric median diameter, D_g and the geometric standard deviation, σ_g. Given that the distribution of the particle

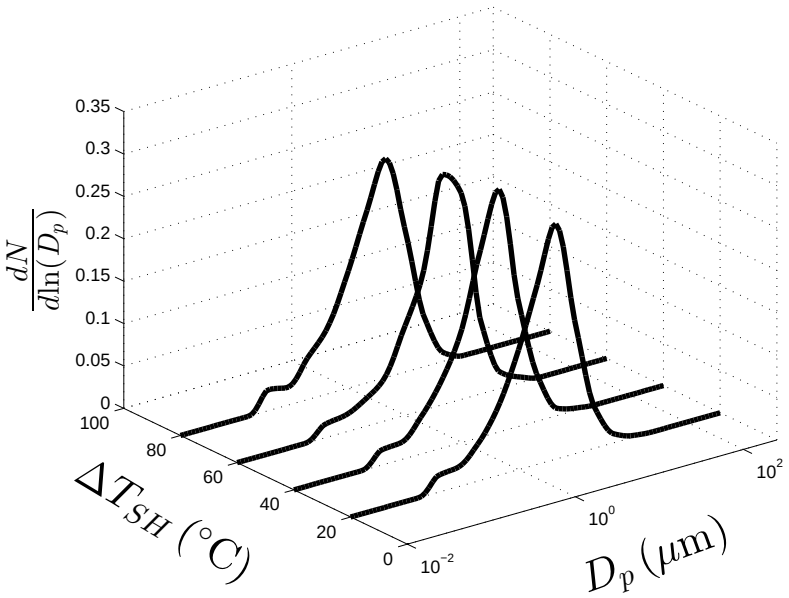

Figure 3.46: Probability functions with $p_r = 17.0$

diameters is log-normal, these two extra parameters are included as is the standard when working with log-normal distributions. These parameters are defined in Equations 3.2 and 3.3.

$$D_g = \frac{\sum \ln D_i}{N} \tag{3.2}$$

$$\sigma_g = \left[\frac{\sum \left[(\ln D_i - \ln D_g)^2 \right]}{N - 1} \right]^{1/2} \tag{3.3}$$

Table 3.2: Centerline diameter summary statistics

p_r (−)	ΔT_{SH} (°C)	μ_{D_p} (µm)	σ_{D_p} (µm)	D_g (µm)	σ_g (−)
0.68	20	2.6	2.1	1.9	2.5
	40	3.3	2.9	2.3	2.6
	60	2.9	2.3	2.1	2.6
	80	(−)	(−)	(−)	(−)
10.2	20	3.2	3.3	2.2	2.6
	40	2.5	2.3	1.7	2.6
	60	2.6	1.9	1.9	2.5
	80	2.9	2.5	2.0	2.6
13.6	20	2.6	3.1	1.6	2.9
	40	2.4	2.3	1.6	2.7
	60	3.0	2.4	2.1	2.6
	80	2.9	2.3	2.0	2.6
17.0	20	2.9	2.9	2.0	2.5
	40	3.6	2.6	2.7	2.4
	60	3.6	2.6	2.7	2.4
	80	2.6	2.2	1.8	2.7

Chapter 4

Discussion of Results

4.1 Adiabatic Void Fraction

An important parameter in the field of dispersed sprays is the void fraction, α. This is a measure of the fraction of the spray cross sectional area occupied by the gas phase. Because the ratio of densities of liquid water to steam are so large, $\rho_l/\rho_g \approx 1600$, a large void fraction can be achieved, even with a relatively small mass fraction of steam and prior to entraining ambient gas. The measurement of the void fraction in dense sprays can become complicated and for this reason, it will be modeled using theoretical predictions.

In order to estimate the unmixed adiabatic void fraction, the mass fraction of steam must first be estimated. The steam quality is estimated by assuming that the initially sub-cooled mixture flashes at the reservoir temperature and the resultant two phase mixture exists at the saturation temperature of the ambient conditions. It is assumed that no heat transfer occurs between the two phases, nor the ambient. For a given initial temperature, T_1, the stream quality can be estimated using Equation 4.1.

$$x = \frac{h_{l,T_1} - h_{l,100\,^\circ\mathrm{C}}}{h_{lg,T_1} + h_{g,100\,^\circ\mathrm{C}} - h_{l,100\,^\circ\mathrm{C}}} \tag{4.1}$$

For an ambient pressure of approximately 1 atm, the saturation temperature of water is 100 °C. Using the saturated steam tables in Moran and Shapiro (2008), these conditions give $h_{f,100^\circ\mathrm{C}} = 419.04\,\mathrm{kJ/kg}$ and $h_{g,100^\circ\mathrm{C}} = 2676.1\,\mathrm{kJ/kg}$; where $h_{l,T}$ represents the enthalpy of saturated liquid at temperature, T, $h_{l,T}$ represents the enthalpy of saturated vapour at temperature, T, and $h_{lg,T}$ represents the latent heat of evaporation at temperature, T,.

The steam quality represents the mass fraction of steam in the two phase mixture. The evaluation of the steam quality depend upon the enthalpy of the sub-cooled liquid as well as the enthalpy of evaporation at the reservoir temperature. The remaining parameters are dependent only upon the saturation temperature of the ambient conditions, which is

taken to be 100 °C. With this quantity known, the void fraction can be estimated using Equation 4.2 from Rice (1987).

$$\alpha = \frac{x\rho_l}{S\rho_g(1-x) + x\rho_l} \tag{4.2}$$

In Equation 4.2, the quantity, S represents the slip ratio. This is the ratio of the gas velocity to the liquid velocity. In order to accurately measure this quantity, detailed measurements of the local velocities of both the continuous and dispersed phase are needed. Due to the difficulties in obtaining these measurements, particularly in dense spays, this quantity will be modeled using correlations found in literature. Bar-Kohany *et al.* (2007) cite a relation for determining the slip ratio of the fluids. This relation was calculated by minimizing the spray momentum with respect to the slip ratio and is shown in Equation 4.3

$$S \equiv \frac{U_g}{U_l} = \left(\frac{\rho_l}{\rho_g}\right)^{1/2} \tag{4.3}$$

With the above relations, the adiabatic void fraction of the spray at each of the tested reservoir temperatures was calculated. These results are shown in Table 4.1. As can be seen, even with a steam quality of only 8%, the void fraction is approximately 78%.

Table 4.1: Steam quality and void fraction of Flash atomized spray

ΔT_{SH} (°C)	$h_{f,T_{\text{reservoir}}}$ (kJ/kg)*	$h_{fg,T_{\text{reservoir}}}$ (kJ/kg)*	x (−)	α (−)
20	503.71	2202.6	0.0159	0.3928
40	589.13	2144.7	0.0385	0.6157
60	675.55	2082.6	0.0595	0.7168
80	763.22	2015.0	0.0804	0.7778

*Source: Moran and Shapiro (2008)

4.2 Velocity results

4.2.1 Radial Profiles of Droplet Velocity

The radial profiles of droplet velocity measured at constant temperatures are shown in Figures 3.1 through 3.4. These figures demonstrate the effect of changing reservoir pressure on the droplet velocity profiles. Each figure contains velocity profiles for all tested pressures for the given reservoir pressure.

Firstly, it can be noted that, in general, the droplet velocity profiles fit an expected Gaussian distribution. This is the type of velocity profile expected of single-phase jets

and is consistent with velocity profiles measured by Yildiz *et al.* (2006) and Zhifu *et al.* (2012). The maximum spray velocity occurs at or in the near vicinity of the jet centerline. At increasing radial positions, the droplet velocities decrease monotonically, in general, towards a minimum at the spray periphery. This general trend is present regardless of the reservoir conditions.

The effect of reservoir pressure on the droplet velocity profiles is shown in these figures. It can be seen that at higher reservoir temperatures, the effect of the pressure ratio on the centerline velocities diminishes. At $\Delta T_{SH} = 20\,^{\circ}\mathrm{C}$, the centerline velocities of the droplets range from $U_z \approx 24\,\mathrm{m/s}$ for $p_r = 6.8\,\mathrm{MPa}$, to $U_z \approx 36\,\mathrm{m/s}$ for $p_r = 17.0\,\mathrm{MPa}$. conversely, with $\Delta T_{SH} = 80\,^{\circ}\mathrm{C}$, the centerline droplet velocities for all tested pressures are within the range of $32 - 35\,\mathrm{m/s}$. The distribution of the droplet velocities also narrows as the radial position is increased. This is evident in all cases except when $\Delta T_{SH} = 80\,^{\circ}\mathrm{C}$, where the centerline droplet velocities are more narrowly distributed than those on the periphery. As the air is entrained, the droplets transfer momentum and begin to slow. The velocity gradients decrease towards the spray periphery, and under all test conditions, the velocities near the outer edge of the spray envelope lie in the $3 - 5\,\mathrm{m/s}$ range.

In most cases, higher reservoir pressure results in a higher droplet velocity, particularly in the vicinity of the jet centerline. This is an expected result, particularly on the jet centerline where the effect of the entrained ambient air is minimized. However, for $\Delta T_{SH} = 80\,^{\circ}\mathrm{C}$, the droplet velocity is narrowly distributed and no clear trend is present. This is particularly true in regions near the jet centerline, with $r = 0 - 15\,\mathrm{mm}$. At this high temperature, the adiabatic void fraction was estimated to be $\alpha_{180^{\circ}\mathrm{C}} = 0.7778$. It is possible that at this temperature, the flow approaches or achieves choked flow. If the two phase flow at the nozzle throat becomes choked, further increases in reservoir pressure will not result in increased throat velocity. Rossmeissl and Wirth (2006) state that the sonic velocity of a two phase mixture is significantly lower than that of wither single phase. They state that the sonic velocity, a_{lg} of a two phase mixture can be determined using the sonic velocity of the liquid phase, a_l and gas phase a_g as well as the fluid densities and the void fraction using Equation 4.4.

$$a_{lg} = \frac{1}{\sqrt{\frac{\alpha}{a_g^2}\left[1 + (1+\alpha)\left(\frac{\rho_l}{\rho_g} - 1\right)\right] + \frac{1-\alpha}{a_l^2}\left[1 + \alpha\left(\frac{\rho_g}{\rho_l} - 1\right)\right]}} \tag{4.4}$$

Using this equation and values of $a_g = 477\,\mathrm{m/s}$ and $a_l = 1547\,\mathrm{m/s}$, as outlined in sectionA, the sonic velocity of the mixture with $\Delta T_{SH} = 80\,^{\circ}\mathrm{C}$ is $a_{lg} = 28.6\,\mathrm{m/s}$. This

calculated value is larger than the predicted sonic velocity. However, it has been found by Zhou *et al.* (2011) that further expansion downstream of the nozzle outlet results in the acceleration of the liquid droplets. Their study found that the maximum velocity of a flashing R404a spray occurred 50 mm downstream of the nozzle outlet, then the velocity decreased along the spray direction.

Firstly, it can be noted that, in general, the droplet velocity profiles fit an expected Gaussian distribution. This is the type of velocity profile expected of single-phase jets and is consistent with the findings reported by Wiltox and Bowen (2002). The maximum spray velocity occurs at or in the near vicinity of the jet centerline. At increasing radial positions, the droplet velocities decrease monotonically, in general, towards a minimum at the spray periphery. A notable characteristic of the velocity profiles is that at both high temperatures and pressures, the droplet velocities near the jet centerline are increasingly uniform. At both lower temperatures and pressure, the deviation of velocities along the jet centerline in noticeably larger.

4.2.2 Velocity Plots

The profile plots included earlier provide insight into the effect of the reservoir conditions on the overall velocity profiles. However, it can be difficult to observe local trends in the data. In order to more accurately depict the effect of reservoir conditions on localized droplet velocities, the droplet velocities at radial locations of $r = 0\,\text{mm}$, $r = 15\,\text{mm}$, and $r = 25\,\text{mm}$ and under various operating conditions were plotted.

Figures 3.9 through 3.12 demonstrate that, as expected and as noted in the velocity profile plots, the pressure ratio has a notable impact on the droplet velocities in the vicinity of the jet centerline. This relation appears strongest at $\Delta T_{SH} = 20\,^{\circ}\text{C}$ and $r = 0\,\text{mm}$. This relation persists until $\Delta T_{SH} = 80\,^{\circ}\text{C}$. At this degree of superheat, there is no clear relation between the pressure ratio and the centerline droplet velocity. These figures also show that towards the spray periphery, droplet velocity shows no discernable correlation to the pressure ratio of the spray. These figures indicate that, within the parameter ranges tested, the pressure ratio of the spray has a positive correlation with droplet velocity, though only near the jet centerline and only at degrees of superheat less than $\Delta T_{SH} = 80\,^{\circ}\text{C}$. This indicates that, for a large portion of the spray cross section at the tested axial position of $z = 150\,\text{mm}$, the droplet velocity shows no clear dependence on the pressure ratio of the spray.

The effect of the degree of superheat on the droplet velocity at various radial locations

is illustrated in Figures 3.13 through 3.16. In the majority of these plots, there is no clear correlation, regardless of the tested pressure ratio or the radial position. Despite the fact that the adiabatic void fraction was estimated to increase from $\alpha \approx 40\%$ at $\Delta T_{SH} = 20\,^{\circ}\mathrm{C}$ to $\alpha \approx 80\%$ at $\Delta T_{SH} = 80\,^{\circ}\mathrm{C}$. This increase in the volume of the dispersed phased demonstrated no clear effect upon the velocity of the distributed phase. Given the large value of the slip ratio calculated earlier, $S = 40.04$, the continuous phase of the spray is assumed to have a considerably larger velocity. Therefore, the effect of the continuous phase velocity on the dispersed phase velocity is minimal, relative to the effect of the operating pressure ratio.

4.3 Long Exposure Images

A qualitative indicator of the effect of the reservoir conditions on the flash atomized spray was obtained using long exposure photographs. These photographs demonstrate the effect of the reservoir conditions on the spray envelope. Figure 3.17 illustrates the spray operating at varying pressure ratios and at a constant degree of superheat of $\Delta T_{SH} = 60\,^{\circ}\mathrm{C}$. Under each condition, the spray operates in a qualitatively similar manner. The spray angle exhibits no discernable change, and the width of the spray envelope remains approximately constant across the range of pressure ratios tested.

With the pressure ratio maintained at 13.6, the spray was tested at a variety of reservoir temperatures. The results are summarized in Figure 3.18. These photographs indicate a distinct qualitative change in the operating conditions of the spray as the reservoir temperature is changed. The spray angle increases with increasing temperature; as does the width of the spray envelope. Another important characteristic revealed by these photographs is that at low degrees of superheat (for $\Delta T_{SH} = 20\,^{\circ}\mathrm{C}$), an intact liquid core appears to exist along the jet center line in the near field region of the nozzle outlet. This is an indication that the energy released via the flashing process was insufficient to fully atomize the spray, thereby leaving a liquid core. At low temperature, the spray appears to operate in the partially shattering regime, as defined by Peter *et al.* (1994). At all higher temperatures, the jet appears to operate in the flare shattering regime.

As shown in the remaining long exposure photographs, the liquid core persists at all tested reservoir pressures, provided that the temperature is sufficiently low. That this liquid core persists along the jet center-line indicates that under the studied operating conditions, the onset of flashing occurs at nucleation sites along the nozzle wall and the flashing occurs primarily from the nozzle wall towards the jet core. It can also be noted that all cases,

even those operating in partially shattering regime, the spray cone is coincident with the nozzle outlet. This is indicative of an internal flashing regime. That is, the onset of the nucleation occurs prior to the nozzle outlet. Given the findings of Park and Lee (1994), providing a nozzle aspect ratio of $L/D = 7$ above which flashing occurs internally, and the large aspect ratio used in the current work ($L/D = 16$), this result is in agreement with published literature. This indicates a two-phase spray is present within the nozzle, prior to the outlet.

The spreading angles of the jet in the near and far-field (θ_n and θ_f, respectively) were measured using the long exposure images at a variety of upstream conditions. In Figure 3.19, the effect of the degree of superheat on each of the spreading angles is illustrated. From this figure, it is clear that the near field spreading angle increases significantly as ΔT_{SH} is increased. In general, it can be seen that the near-field spreading angle is larger than the far-field spreading angle. This indicates a curvature in the jet, as the rapid spreading in the near-field lessens downstream. For $\Delta T_{SH} = 30\,^{\circ}\mathrm{C}$, however, θ_n and θ_f are of similar values. This indicates a relatively constant spreading rate at low degrees of superheat. As ΔT_{SH} is increased, θ_n becomes larger. The rate of increase of θ_n, however, is lower at high values of ΔT_{SH}, indicating that the dependance of θ_n on ΔT_{SH} decreases at high temperatures. This finding is consistent with the work of Kamoun *et al.* (2010). Their study noted that spray angle increased as the degree of superheat was increased, but at high degrees of superheat, the spray angle began to decrease. In Figure 3.19, the far-field angle remains relatively constant as ΔT_{SH} is increased. This indicates that sufficiently far downstream, the increased spreading caused by the higher degrees of superheat is no longer evident.

In Figure 3.20, the near and far field angles were measured as the pressure ratio of the spray was altered. From this figure, it can be seen that both θ_n and θ_f appear relatively robust with respect to changes in p_r. For all degrees of superheat except $\Delta T_{SH} = 20\,^{\circ}\mathrm{C}$, the near-field angle is significantly larger than the far-field angle. However, as the pressure ratio is increase, there is only a minimal change in the values of both θ_n and θ_f.

4.4 Data Rate Profiles

The data rate of the PDPA system was measured and the radial profiles of its value are shown in Figures 3.25 through 3.28. These normalized radial profiles of the PDPA data rate were collected at various degrees of superheat with a constant pressure ratio of 17.0. From these figures, it is clear that the maximum data rate does not occur on the jet centerline,

where the maximum spray density is expected. Instead, the data rate generally peaks in the region of $r = 10 - 20\,\text{mm}$. Because the flash atomizer produces such a dense spray, the PDPA system does not function as well when measuring near the spray centerline. The high spray density obscures the signal as it travels to the receiver. Therefore, there is an optimum region where the spray density remains high, but the visibility of the receiver is unobscured. From the figures presented, this region exists in the region of $r = 10 - 20\,\text{mm}$. Beyond this region, though the visibility increases, the low spray density results in an ever decreasing data rate.

It can be seen that, in all cases, the data rate at the spray periphery is decreasing as the radial position is increased. In Figure 3.25 with $\Delta T_{SH} = 20\,^{\circ}\text{C}$, the data falls below 10% of the maximum at $r = 25\,\text{mm}$. Measurements beyond this point were not possible due to the prohibitively low data rates and limited experimental release time. For higher values of ΔT_{SH}, It was possible to obtain measurement up to $r = 30\,\text{mm}$ before the data rate became too low. This supports the earlier conclusion that the spray envelope decreases as the temperature is reduced.

4.5 Diameter Results

An important aspect in the field of atomization is the size of the droplets produced. It is also important to quantify the spatial variance of the diameters as well as the distribution of the diameter sizes. To this end, the PDPA proved a valuable measurement device due to its ability to acquire spatially resolved diameter measurements of the spray.

4.5.1 Diameter Profiles

The spatial distributions of D_{32} under a variety of measurement conditions were obtained. Figures 3.29 through 3.32 demonstrate the radial profiles of D_{32} with each figure representing operation at a constant pressure ratio. From these figures, there are a number of apparent trends.

Firstly, it is noted that, in general, the values of D_{32} are smaller at smaller radial positions. The general trend in these figures is for D_{32} to increase towards the spray periphery. There are several possible reasons for this occurrence. The nozzle geometry may impact the diameter profiles downstream. Another possible explanation involves the ambient air that is entrained into the jet, as stated by Wiltox and Bowen (2002). Given that the spray cools as it enters the ambient a conservative estimate of the Reynolds number can be obtained by evaluating parameters at the mean of the ambient and saturation temperatures:

$$Re = \frac{\rho V D_p}{\mu} = \frac{\left(1.09 \frac{\text{kg}}{\text{m}^3}\right)\left(5 \frac{\text{m}}{\text{s}}\right)(3\mu\text{m})}{1.95 \times 10^{-5} \frac{\text{Ns}}{\text{m}^2}} = 0.84 \tag{4.5}$$

In the region of the spray periphery, the Reynolds number of the droplets is approximately 0.84. Creeping flow occurs for flow with $Re << 1$. Under the measured conditions with $Re = 0.84$, it is assumed that the flow is not creeping. For non-creeping laminar flow, the drag force on an object varies as the projected area, in the case of a sphere, $F \propto D_p^2$. The mass of a spherical droplet varies with the volume, $m \propto D_p^3$. Therefore, the drag force per unit mass, F/m for these water droplets is:

$$\frac{F}{m} \propto \frac{D_p^2}{D_p^3} = \frac{1}{D_p} \tag{4.6}$$

It can therefore be seen that the force per unit mass is larger for larger diameter particles. As the air is entrained and migrates towards the jet centerline, low inertia droplets will be disproportionately affected. Given the relatively low inertia of the low mass droplets and the higher drag force per unit mass of small particles, this effect would cause a relative abundance of smaller droplets towards the jet centerline. In order to determine the process by which the diameter profiles observed are formed, further measurements at axial locations closer to the nozzle outlet must be made. With the equipment limitations imposed, this was not possible in the current study.

Another trend apparent in the four figures presented is that the variation between the centerline and peripheral D_{32} values becomes smaller as the reservoir pressure is increased. It can be noted that the highest pressure studied ($p_r = 17.0$), the value of D_{32} never exceeds 40 µm, this is approximately one third of the maximum value obtained with $p_r = 6.8$. It can be concluded that under high pressures, the atomization of the spray is increasingly uniform.

Given the variation between the centerline and peripheral values of D_{32}, Figures 3.29 through 3.32 obscure the local trends in the profile in the region near the jet centerline. In order to better observe the data trends in this region, Figures 3.33 through 3.36 use a scaled ordinate in order to focus on the trends at low radial positions. The trends observed in these figures mirror those evident in Figures 3.29 through 3.32. Notably, the diameter distribution become increasingly uniform at higher pressure ratios. Figures 3.29 through 3.32 make apparent, however, that at pressure ratios of 10.2 and 13.6, there is a local maximum of D_{32} at $r = 0$ mm for $\Delta T_{SH} = 20\,^{\circ}$C. This peak is not apparent at pressure ratios of 6.8 or 17. Based on the previous analysis of the long exposure photographs in Section 4.3,

it is likely that this local maximum of D_{32} is the result of the greater axial reach of the intact liquid core present when $\Delta T_{SH} = 20\,^{\circ}\mathrm{C}$. Given that the flashing process does not atomize the spray completely under these conditions, the remaining liquid core is left to break up under the action of shear forces downstream of the nozzle. The radial profiles indicate that this results in a localized region of relatively large values of D_{32}. Under the pressure ratios of 6.8 and 17 this effect is not observed. This is perhaps the result of the liquid core breaking up upstream of the measurement plane. At low pressure, this may be due to the lower inertia of the spray, whereas for $p_r = 17.0$, the increased pressure may result in enhanced shear forces on the jet core. Measurements along the centerline at axial locations farther upstream may assist in illuminating the cause of this observed peak.

In order to more clearly observe the effect of the degree of superheat on the radial profiles od D_{32}, Figures 3.37 through 3.40 demonstrate the same radial profiles of D_{32} but presented in figures of constant temperature. The trends observed earlier hold in this presentations. The largest values appear at the spray periphery, but the magnitude of the maximum value decreases with increasing degree of superheat. Notably however, is the fact that for $\Delta T_{SH} = 20\,^{\circ}\mathrm{C}$, there is no data beyond $r = 25\,\mathrm{mm}$. This is consistent with the findings of the long exposure photographs. The spray envelope decreases as the degree of superheat decreases. As such, PDPA measurements were not feasible beyond $r = 25\,\mathrm{mm}$ for $\Delta T_{SH} = 20\,^{\circ}\mathrm{C}$. Also worth noting is that the radial profile of D_{32} for $\Delta T_{SH} = 80\,^{\circ}\mathrm{C}$ exhibits minimal variation between the centerline and peripheral values of D_{32}.

With a magnified ordinate, the radial profiles at constant temperature are reproduced in Figures 3.41 through 3.44. The local maxima noted earlier and attributed to the intact liquid core are visible in Figure 3.41, with $\Delta T_{SH} = 20\,^{\circ}\mathrm{C}$. As the degree of superheat is increased, the uniformity of the profiles operating under various pressure ratios increased. This is particularly apparent in the region of $r = 0 - 15\,\mathrm{mm}$ with $\Delta T_{SH} = 80\,^{\circ}\mathrm{C}$. In this area, the effect of pressure on the radial profile of D_{32} is imperceptible. This is consistent with the effect of the degree of superheat on the radial profiles of droplet velocities. At high degrees of superheat, the spray properties appear to be robust with respect to changes in the operating pressure ratio.

The above findings relating to D_{32} are reflected in the summary in Table 3.1.

4.6 Probability Density Functions

The effect of the pressure ratio on the probability density function is shown in Figure 3.45. This figure contains data collected at a constant degree of superheat of $\Delta T_{SH} = 60\,^{\circ}\mathrm{C}$ and

variable pressure ratio. In all cases, the peak of the distribution occurs in the region of $2 - 4\,\mu\text{m}$. The distributions appear unimodal about the peak value. However, there is a small secondary bump occurring at approximately $0.1\,\mu\text{m}$. This secondary peak is present at all pressure ratios tested. From this figure, it can be concluded that the pressure ratio of the spray does not have any discernable effect on the diameter distribution. This conclusion is supported by the data in Table 3.2. Both the mean diameter and the geometric median diameter vary by approximately $1\,\mu\text{m}$ as the pressure ratio is changed. Furthermore, the value of the geometric standard deviation is consistent at all pressure ratios. The geometric mean diameter is a dimensionless measure of the distribution of the data. That this quantity does not vary significantly indicates that the changing pressure ratio has a minimal impact on the diameter distributions measured.

Figure 3.46 depicts the effect of a variable degree of superheat on the PDFs of the droplet diameters measured at a constant pressure ratio of $p_r = 17.0$. Again, the PDFs have a primary peak at approximately $2-4\,\mu\text{m}$. It can be seen, however, that the secondary peak at approximately $0.1\,\mu\text{m}$ becomes larger at $\Delta T_{SH} = 80\,^{\circ}\text{C}$. This result is consistent with work done by Batenin *et al.* (2010). In their study of a flash atomized water jet with a coaxial air flow, they noted a bimodal distribution of the droplet diameters. Their study produced PDFs with a peak at approximately $0.1 - 0.2\,\mu\text{m}$ and another at approximately $1 - 3\,\mu\text{m}$. This is consistent with the findings in Figure 3.46. However, Batenin *et al.* noted a mass fraction of approximately 50% at diameters less than $1\,\mu\text{m}$. This is likely due to the fact that their experiments were performed with $\Delta T_{SH} = 140$ and $p_r \approx 80$. This high degree of superheat creates a more energetic flashing of the spray as the pressure drops in the nozzle. However, Batenin *et al.* note that the presence of this secondary peak becomes particularly apparent at $\Delta T_{SH} \approx 70\,^{\circ}\text{C}$. They note that colder jets exhibit unimodal distributions. Though the current work is limited in the degree of superheat attainable, the results obtained are consistent with the literature.

Chapter 5

Conclusions

This study investigated the effects of the operating conditions of a flash atomized spray on the droplet characteristics downstream. In order to obtain concurrent velocity and diameter results, a PDPA system was used. Spatially resolved data was obtained by mounting the PDPA system on a motorized three axis traverse. The degree of superheat and the operating pressure ratio of the spray were systematically altered in order to measure the effect of each on the droplet characteristics of the spray.

The velocity profiles were measured using the PDPA system. The results were consistent with the literature and exhibited a Gaussian shape. It was found that the pressure ratio of the system had a positive correlation with the droplet velocity, though only in the region near the jet centerline. Near the jet periphery, the effect of the pressure ratio was indeterminate. It was also found that the degree of superheat had no discernable impact on the droplet velocity. Despite the increased mass fraction of vapour in the spray as the degree of superheat was increased, the droplet velocity remained relatively unaffected. At high degrees of superheat, however, it was also found that, even on the jet centerline, the pressure ratio had no measurable effect on the droplet velocity. At high degrees of superheat, the void fraction of the spray increases. As this happens, the sonic velocity of the spray decreases to a value less than that of either pure vapour or liquid. The robustness of the droplet velocity with respect to pressure ratio at $\Delta T_{SH} = 80\,^{\circ}\mathrm{C}$ is indicative of choked flow.

Long exposure photographs were taken and used in order to qualitatively determine the effect of the inlet conditions ion the spray produced. The 30 s exposure photographs revealed that the spray angle and envelope both increase as the degree of superheat is elevated. This finding was corroborated when plotting the radial profiles of the PDPA data rate. At $\Delta T_{SH} = 20\,^{\circ}\mathrm{C}$, the data rate became prohibitively low at $r = 25\,\mathrm{mm}$ whereas at

higher degrees of superheat, measurements were made up to $r = 30\,\text{mm}$. Furthermore, it was found that at low degrees of superheat, $\Delta T_{SH} = 20\,^{\circ}\text{C}$, the flashing process fails to completely atomize the spray. As a result there exists an intact liquid core along the jet centerline. It was noted that the effect of this liquid core persisted downstream and it's influence resulted in elevated values of D_{32} at the measurement plane of $z = 150\,\text{mm}$.

As the degree of superheat was increased, the atomization of the spray became increasingly uniform. It was noted that with $\Delta T_{SH} = 80\,^{\circ}\text{C}$, the variation between the centerline and peripheral values of D_{32} was minimized, with centerline values of $D_{32} \approx 8\,\mu\text{m}$ and peripheral values of $D_{32} \approx 10 - 20\,\mu\text{m}$. At lower degrees of superheat, this variation increases significantly.

Overall, it can be concluded that at sufficiently high degrees of superheat, the characteristics of the flash atomized spray are robust with respect to changes in the operating pressure ratio.

The data collected indicates that, under the tested conditions, the flashing process initiates inside the nozzle. This results in a two-phase flow inside the nozzle which, at high degrees of superheat, appears to become choked. Based on the images collected and the data obtained using the PDPA system, it was found that the flash atomized spray produces increasingly uniform characteristics as the degree of superheat was increased. The droplet velocities show minimal dependence on the pressure ratio, provided that the degree for superheat is sufficiently high. It was posited that this indicates a choked two-phase flow in the nozzle throat. The radial profile of droplet diameters also becomes increasingly uniform at high degrees of superheat. The pressure ratio of the spray has only a minimal impact on the droplet diameters when the degree of superheat is large. This characteristic is beneficial in power generating applications where pressure fluctuations due to varying load are common.

5.1 Future Work

The experiments discussed thus far have dealt with the flash atomization of a single-phase, single-component fluid; namely, water. However, many industrial applications of flash atomization involve the flashing of a fluid containing dispersed solids in suspension. This can be done with coal or other long chain hydrocarbons. This type of system is beneficial in that the emulsified fluid facilitates transport via pipeline. Furthermore, it may be possible to predetermine the fuel diameter in the spray by tailoring the suspended particles to the desired application. Such systems may provide increased usability and efficiency of heavy

hydrocarbons which were previously under utilized due to economic impediments. However, the research and development of such systems is complicated by a complex and poorly understood physical mechanism and difficulties in obtaining reliable measurements. Future work in this area could be oriented towards applying these methodology to suspended fuel solutions.

As a first investigation into flash atomization of suspended fuel particles, glass spheres were mixed with the water in the pressure vessel and heated to super critical temperatures. The manufacturer's specified average diameter of the glass spheres was 20 µm. Given the large disparity between the diameter of the glass spheres and the previously observed droplet diameters under flashing conditions, a bimodal diameter distribution was expected. However, the presence of the glass spheres may complicate the interfacial physics of the flashing process.

The measurement system remained unchanged from the previous tests. In order to minimize the buoyancy effects of the glass spheres, the suspension was made and left to settle for several hours. This allowed for only the approximately neutrally buoyant glass spheres to be used in the flashing experiment.

The PDPA system was once again used in order to measure the droplet and particle diameters in the flashing spray. With $\Delta T_{SH} = 40\,^{\circ}\mathrm{C}$ and $PR = 13.6$, the glass sphere suspension was flash atomized and measured with the PDPA system. The PDF of the centerline diameters of the obtained results is shown in Figure 5.1. This distribution is overlayed on the results obtained using only water at the same conditions. The results are also summarize in Table 5.1.

Table 5.1: Comparison of suspension with single component spray.
$PR = 13.6$, $\Delta T_{SH} = 40\,^{\circ}\mathrm{C}$

Type of Release	μ_{D_p} (µm)	σ_{D_p} (µm)	D_g (µm)	σ_g (−)	D_{32} (µm)
Water	2.4	2.3	1.6	2.7	8.1
Glass Sphere Suspension	10.4	11.9	6.2	3.0	43.8

From the figure, it is clearly visible that the expected bimodal distribution is not present. However, the influence of the glass spheres is observable in the fact that, though unimodal, the diameter distribution with glass spheres is significantly shifted towards larger diameters. The shape of the distribution remains relatively unchanged, save for the fact that the

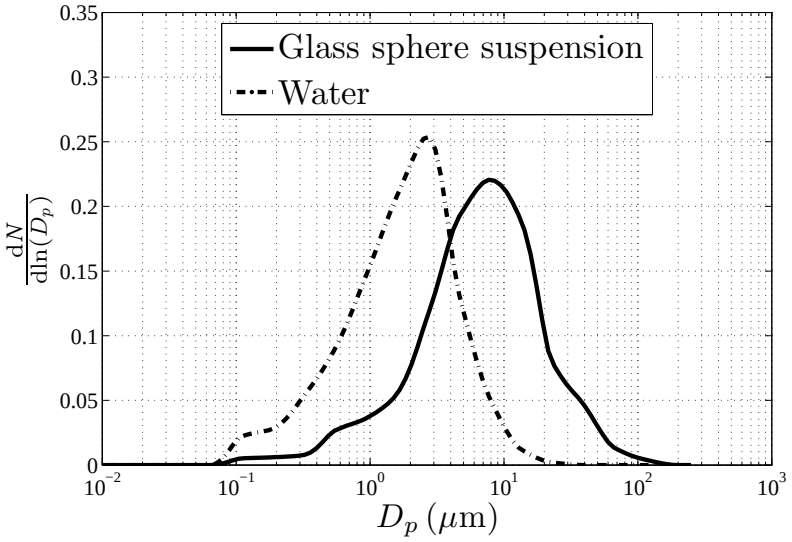

Figure 5.1: Comparison of glass sphere suspension spray and water spray

diameter sizes are, in general, larger. From this figure, it is unclear whether the glass spheres and water droplets are distinct entities within the spray or if they have amalgamated.

Table 5.1 clearly indicates that the measured droplet size and D_{32} are significantly larger with the addition of the glass spheres to the spray. Given that the geometric standard deviations of the two release types are of similar magnitude, the dispersion of the data about their respective geometric median diameters are approximately equal. This indicates, as is visible in Figure 5.1, that the shape of the distribution remains relatively unchanged.

Unfortunately, a detailed investigation into the characteristics of the glass sphere suspension spray is not possible with the measurement system used. Firstly, the presence of the glass spheres increased the opacity of the spray significantly. As such, the data rates of the PDPA system were reduced, thereby limiting the number of measurements possible during a single release. Secondly, and most importantly, the index of refraction of the glass spheres is not equal to that of the water droplets. As is evident in Equation 2.2, the index of refraction of the measured particles is used in order to determine the particle diameter. This disparity in the index of refraction renders the accurate measurement of the diameters of the two components intractable using the current system.

In order to further study the phenomenon of the flash atomization of a glass sphere in water suspension, adjustments must be made to the measurement system. A possible solution is to place a fluorescent dye into either the glass spheres or water. Then, using selective filters in the receiver, the signal from the component with the fluorescent dye can

be attenuated, thereby leaving only the Doppler burst corresponding to the unaltered component. However, In order to obtain concurrent measurements of both the water droplets and the glass spheres, an additional PDPA receiver will be required.

Alternatively, a distinct measurement system may offer improved suitability to the problem. As was found by Yildiz *et al.* (2004), the use of particle image velocimetry (PIV), is possible (though not without difficulty) in flashing sprays. A PIV system could be used in order to measure the velocities of both the water droplets and glass spheres. The benefit of using a PIV system lies in the fact that the system returns a vector field of velocity measurements as opposed to the single point measurement provided by the PDPA. However, PIV does not provide particle diameter measurements, which are of crucial importance in atomization systems. In order to obtain diameter measurements, rapid exposure photographs using a long working distance microscope objective and a pulsed laser as a light source may be used. The high spray density may complicate the use of such a system, but, if need be, the release rate of the suspension can be limited in order to allow for accurate diameter measurements.

The field of flash atomization is active in the research community, and given the increased interest and investment in unconventional fuels, further advances in the understanding and implementation of such systems are undoubtedly forthcoming.

References

[1] P.G. Aleiferis and Z.R. van Romunde. An analysis of spray development with iso-octane, n-pentane, gasoline, ethanol and n-butanol from a multi-hole injector under hot fuel conditions. *Fuel*, 105:143–168, March 2013.

[2] T. Bar-Kohany, I. Sher, and E. Sher. Choked flow of a bubbly mixture through an effevescent and flash boiling atomizer: A theoretical approach. *Atomization Spray*, 17:431–449, 2007.

[3] V.M. Batenin, V.I. Zalkind, Y.A. Zeigarnik, and V.L. Nizovski. Some aspects of atomization of superheated water by flashing. *Dokl Phys*, 55(3):115–118, March 2010.

[4] P.J. Bowen. *Flashing liquid jets and two-phase dispersion, a review.* 2002.

[5] C.E. Brennen. *Fundamentals of multiphase flow.* Cambridge University Press, 2005.

[6] J Dernotte, C Hespel, and S Houill. Influence of fuel properties on the diesel injection process in nonvaporizing conditions. 22(6):461–492, 2012.

[7] A.K. El-Fiqi, N.H. Ali, H.T. El-Dessouky, H.S. Fath, and M.A. El-Hefni. Flash evaporation in a superheated water liquid jet. *Desalination*, 206(1-3):311–321, February 2007.

[8] M.E. Ferreira, C.F. Teixeira, C.J. Bates, and P.J. Bowen. Detailed investigation of the influence of fluid viscosity on the performance characteristics of plain-orifice effervescent sprays. *Atomization spray*, 11:107–124, 2001.

[9] E. Hervieu and T. Veneau. Experimental determination of the droplet size and velocity distributions at the exit of the bottom discharge pipe of a liquefied propane storage tank during a sudden blowdown. *J Loss Prevent Proc*, 9(6):413–425, 1996.

[10] J. Jedelsky and M. Jicha. Spatially and temporally resolved distributions of liquid in an effervescent spray. *Atomization spray*, 22(7):603–626, 2012.

[11] H. Kamoun, G. Lamanna, B. Weingand, and J. Steelant. High-speed shadowgraphy investigations of superheated liquid jet atomisation. In *ILASS-Americas 22nd Annual Conference on Liquid Atomization and Spray Systems*, number May, 2010.

[12] W. Kim, T. Yu, and W. Yoon. Atomization characteristics of emulsified fuel oil by instant emulsification. *J Mech Sci Technol*, 26(6):1781–1791, June 2012.

[13] N.I. Kolev. *Multiphase flow dynamics 2: Thermal and mechanical interactions*. Springer, 2005.

[14] Dancho Konstantinov, Richard Marsh, Phil J. Bowen, and Andrew Crayford. Effervescent atomization for industrial energy-technology review. *Atomization spray*, 20(6):525–552, 2010.

[15] R. Lecourt and B. Philippe. Spray velocity and drop size measurements in flashing conditions. *Atomization Spray*, 19(2):103–133, 2009.

[16] G. Li, J. Cao, M. Li, Y. Quan, and Z. Chen. Experimental study on the size distribution characteristics of spray droplets of DME/diesel blended fuels. *Fuel Process Technol*, 104:352–355, December 2012.

[17] M.J. Moran and H.N. Shapiro. *Fundamentals of engineering thermodynamics*. John Wiley and Sons, Inc., 2008.

[18] S.Y. Park, B.S.; Lee. An experimental investigation of the flash atomization mechanism. *Atomization Spray*, 4:159–179, 1994.

[19] R. Payri, F.J. Salvador, J. Gimeno, and J. De La Morena. Analysis of diesel spray atomization by means of a near-field visualization technique. *Atomization spray*, 21(9):753–774, 2012.

[20] E.M. Peter, A. Takimoto, and Y. Hayashi. Flashing and shattering phenomena of superheated liquid jets. *JSME Int J*, 37(2), 1994.

[21] M.A. Rahman, M. Balzan, T. Heidrick, and B.A. Fleck. Effects of the gas phase molecular weight and bubble size on effervescent atomization. *Int J Multiphas Flow*, 38(1):35–52, January 2012.

[22] C K Rice. The effect of void fraction correlation and heat flux assumption on refrigerant charge inventory predictions. *ASHRAE Transactions*, 93:341–367, 1987.

[23] M. Rossmeissl and K. Wirth. Critical mass-flow in orifice-nozzles at the disintegration of superheated liquids. In *ASME Conference Procedings*, pages 1381–1388, 2006.

[24] U K Sarkar and K Ramamurthi. Flow visualization of sprays formed by bubbly, slug, and annular flows in an effervescent atomizer. 14:397–408, 2007.

[25] E. Sher, T. Bar-Kohany, and A. Rashkovan. Flash-boiling atomization. *Prog Energ Combus Sci*, 34(4):417–439, August 2008.

[26] E. Sher and M. Zeigerson-Katz. Spray formation by flashing of a binary mixture: An energy balance approach. *Atomization Spray*, 6:447–459, 1996.

[27] M.R. Vetrano, A. Simonini, J. Steelant, and P. Rambaud. Flashing jet characterization by non intrusive laser based measurement technique. In *16th Int Symp on Applications of Laser Techniques to Fluid Mechanics*, pages 9–12, 2012.

[28] D. Yildiz, P. Rambaud, and Buchlin J.M. Van Beeck, J.V.B. Characterization of superheated liquid jet atomisation with phase Doppler anemometer (PDA) and high-speed imaging. *2006 ASME Joint U.S. - European Fluids Engineering Summer Meeting*, pages 1–10, 2006.

[29] D. Yildiz, J.V.B. Van Beeck, and M.L. Riethmuller. Feasibility exploration of laser-based techniques for characterization of a flashing jet. *Part Part Syst Char*, 21(5):390–402, December 2004.

[30] J. Yu, Z. Yu-sheng, and M. Elkelawy. Spray and Combustion Characteristics of HCCI Engine Using DME / Diesel Blended Fuel by Port- Injection. *SAE Technical Paper 2010-01-1485*, 2010.

[31] J. Yu, Y. Zhang, G. Jiang, and Q. Kui. An experimental study on steady flash boiling spray characteristics of DME / Diesel blended fuel. *SAE Technical Paper 2010-01-0879*, 2010.

[32] T.U. Yu and J.M. Beer. Secondary atomization of coal-water fuels for gas turbine applications. Technical report, M.I.T. Energy Lab, 1988.

[33] J. Zhang, D. Jiang, Z. Huang, T. Obokata, S. Shiga, and M. Araki. Experimental study on flashing atomization of methane/liquid fuel binary mixtures. *Energ Fuel*, 19(5):2050–2055, September 2005.

[34] Z. Zhifu, W. Weitao, C. Bin, W. Guoxiang, and G. Liejin. An experimental study on the spray and thermal characteristics of R134a two-phase flashing spray. *Int J Heat Mass Tran*, 55(15-16):4460–4468, July 2012.

[35] Z. Zhou, W. Wu, G. Wang, Z. Gong, B. Chen, Y. Wang, and L. Guo. Thermal characteristics of flashing spray of volatile R134a cryogens. *ASME Conference Procedings*, 2011:649–656, 2011.

Appendix A

Speed of Sound Calculations

A.1 Speed of Sound in Water

$$c_p - c_v = \nu \frac{T\beta^2}{\kappa}$$

Properties evaluated at 100 °C (Source: Moran and Shapiro (2008)):

$$c_p = 4.220\,\mathrm{kJ/kg \cdot K}$$
$$\beta = 4.578 \times 10^{-4}\,\mathrm{K^{-1}}$$
$$\kappa = 4.418 \times 10^{-10}\,\mathrm{m^2/N}$$
$$\nu = 1.0435 \times 10^{-3}\,\mathrm{m^3/kg}$$

$$c_v = (4.220\,\mathrm{kJ/kg \cdot K}) - \left(\frac{1.0435\,\mathrm{m^3}}{\mathrm{kg}}\right)(373\,\mathrm{K})\left(\frac{4.578 \times 10^{-4}}{\mathrm{K}}\right)^2\left(\frac{\mathrm{N}}{4.418 \times 10^{-10}\,\mathrm{m^2}}\right)$$
$$c_v = 4.041\,\mathrm{kJ/kg \cdot K}$$

The speed of sound is calculated using the following relation

$$a_l = \sqrt{\frac{k\nu}{\kappa}}$$

with $k = c_p/c_v = 1.044$ gives

$$a_l = \sqrt{\frac{(1.044)(1.0435 \times 10^{-3})\,\mathrm{m^3\,N}}{4.418 \times 10^{-10}\,\mathrm{m^2\,kg}}}$$
$$a_l = 1\,547\,\mathrm{m/s}$$

A.2 Speed of Sound in Steam

$$c_v = c_p - R$$

With the following properties

$$\begin{aligned} R &= \left(\frac{8.314\,\text{kJ}}{\text{kmol}\,\text{K}}\right)\left(\frac{\text{kmol}}{18.02\,\text{kg}}\right) \\ R &= 0.4614\,\text{kJ/kg}\cdot\text{K} \end{aligned}$$

$$\begin{aligned} c_p = &\left(\frac{0.4614\,\text{kJ}}{\text{kg}\,\text{K}}\right)(4.070 - 1.108\times10^{-3}(373\,\text{K}) + 4.152\times10^{-6}(373\,\text{K})^2 \\ &- 2.964\times10^{-9}(373\,\text{K})^3 + 0.807\times10^{-12}(373\,\text{K})^4) \\ c_p &= 1.890\,\text{kJ/kg}\cdot\text{K} \end{aligned}$$

Using these results,

$$\begin{aligned} c_v &= 1.890\frac{\text{kJ}}{\text{kg}\,\text{K}} - 0.4614\frac{\text{kJ}}{\text{kg}\,\text{K}} \\ c_v &= 1.429\,\text{kJ/kg}\cdot\text{K} \end{aligned}$$

This gives $k = c_p/c_v = 1.323$. Using ideal gas relations, the speed of sound can be found:

$$\begin{aligned} a_g &= \sqrt{kRT} \\ a_g &= \sqrt{(1.323)\left(\frac{0.4614\,\text{kJ}}{\text{kg}\,\text{K}}\right)(373\,\text{K})} \\ a_g &= 477\,\text{m/s} \end{aligned}$$

Appendix B

Heat Transfer in the Nozzle Assembly

$$T_e = T_s - (T_s - T_i)\exp\left[\frac{-hA_s}{\dot{m}c_p}\right] \tag{B.1}$$

T_i	Inlet temperature
T_e	Exit temperature
T_s	Surface temperature
h	Convective heat transfer coefficient
A_s	Surface area
$\dot{m}$	Mass flow rate
c_p	Specific heat

Estimate of mass flux: $\dot{m} = 0.01\,\mathrm{kg/s}$

$$\begin{aligned} D_{\text{pipe}} &= 0.0035\,\mathrm{m} \\ V_{\text{pipe}} &= \frac{4\dot{m}}{\rho\pi D_{\text{pipe}}^2} = 1.0851\,\frac{\mathrm{m}}{\mathrm{s}} \\ Re &= \frac{\rho V_{\text{pipe}} D_{\text{pipe}}}{\mu} = \frac{(957.9\frac{\mathrm{kg}}{\mathrm{m}^3})\,(1.0851\frac{\mathrm{m}}{\mathrm{s}})\,(0.0035\mathrm{m})}{2.82\times10^{-4}\frac{\mathrm{kg}}{\mathrm{ms}}} = 12\,901 \end{aligned}$$

Given the large value of Re, the flow is expected to be turbulent. The proper relations for this flow were chosen:

$$\begin{aligned} f &= (0.790\ln[Re] - 1.64)^{-2} = 0.0293 \\ Nu &= 0.125 f Re Pr^{1/3} = 57.0 \\ h &= \frac{Nu\,k}{D} = \frac{(57.0)\,(0.679\frac{\mathrm{W}}{\mathrm{mK}})}{0.0035\mathrm{m}} = 11\,064\frac{\mathrm{W}}{\mathrm{m}^2\mathrm{K}} \end{aligned}$$

The outlet temperature is determined using Equation B.1 for a variable surface temperature. It was found that for a maximum deviation of 10 °C between the inlet temperature

and the surface temperature, the outlet temperature varies by less than 5 °C, as shown in Figure B.1

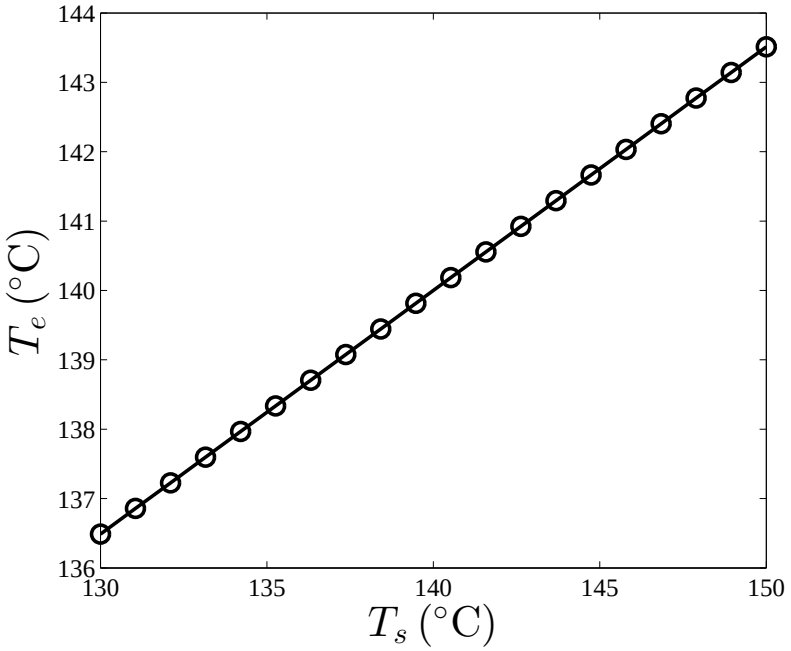

Figure B.1: Effect of surface temperature on outlet temperature.